# LARGE-SCALE SIMULATION OF THE EFFECTS OF CLIMATE CHANGE ON RUNOFF EROSION FOLLOWING EXTREME WILDFIRE EVENTS

By

GREGORY KENNETH GOULD

A thesis submitted in partial fulfillment of
the requirements for the degree of

MASTERS OF SCIENCE IN CIVIL ENGINEERING

WASHINGTON STATE UNIVERSITY
Department of Civil and Environmental Engineering

DECEMBER 2013

To the Faculty of Washington State University:

The members of the Committee appointed to examine the thesis of GREGORY KENNETH GOULD find it satisfactory and recommend that it be accepted.

_____
Jennifer Adam, Ph.D., Chair

_____
Michael Barber, Ph.D.

_____
Keith Cherkauer, Ph.D.

_____
Peter Robichaud, Ph.D.

# ACKNOWLEDGMENT

This research was supported through the State of Washington Water Research Center, the U.S. Department of Agriculture, and Washington State University. Assistance in writing the enclosed manuscript was provided by Jennifer Adam.

I thank my committee for their insight and guidance that helped shape my research into something meaningful. Especially, I am grateful for Jennifer Adam's expertise that made much of this research possible and giving me the opportunity to study at WSU. Also, I am thankful for Mike Barber, for his feedback and collaboration on many aspects of this research. Many thanks go to Keith Cherkauer for his help with providing the model framework. And I thank Pete Robichaud for the great experience and insight on how to incorporate fire into the modeling framework. For all of my committee, I am grateful for their effort and willingness to help.

I would like to thank Kirti Rajagopalan, Keyvan Malek, and Lili Wang for their help in training me in VIC and VIC-WEPP. Also, many thanks go out to Mingliang Liu, Joe Wagenbrenner, and Chad Warren for their collaboration in their technical expertise and contributions. I also thank the Multi-Scale Land Surface Hydrology (MSLSH) Group and the Department of Civil and Environmental Engineering at Washington State University for providing a great place to learn and grow. Finally, I would like to thank for family who have been a constant support through my collegiate years.

LARGE-SCALE SIMULATION OF THE EFFECTS OF CLIMATE CHANGE ON RUNOFF EROSION FOLLOWING EXTREME WILDFIRE EVENTS


Abstract

by Gregory Kenneth Gould, M.S.
Washington State University
December 2013

Chair: Jennifer Adam

Across the western U.S., there is clear concern for increases in wildfire occurrence, severity, and post-fire runoff erosion due to projected climate changes. The first objective for this study is to advance the capability to simulate post-fire runoff erosion at scales larger than a single hillslope to examine the relative sensitivity of erosion to wildfire and climate change. The second objective is to advance the scientific understanding of the interactions between climate, hydrologic processes, fire severity, and post-fire erosion.

The Variable Capacity Infiltration-Water Erosion Prediction Project (VIC-WEPP) model, a newly-developed physically-based modeling framework combining large-scale hydrology with hillslope-scale runoff erosion, is applied over the Salmon River Basin (SRB) in central Idaho. Rather than implementing WEPP over all hillslopes within the SRB, a representative hillslope approach is applied. For future scenarios, only meteorological impacts on post-fire erosion are considered; changes in future fire occurrence or burn severity are not incorporate. The assessment compares pre- and post-fire sediment yields from the VIC-WEPP model with a web-based tool that uses a similar approach, Disturbed WEPP.

Nash Sutcliffe efficiency values over the SRB for VIC modeled simulated streamflow over the calibration (evaluation) period are 0.88 (0.83) and 0.96 (0.93) for daily and monthly time steps, respectively. Streamflow results show an earlier shift in peak flow by one to two months for future climate scenarios. Timing of peak flow shifted to earlier in the season by an average of 26 days for all average future streamflow fire severity conditions. The magnitude of peak flow increased by an average of 18% immediately after each increase in simulated fire severity. For yield change due to wildfire, individual model grid cells range from 0 t $ha^{-1}$ to 927 t $ha^{-1}$. The range of yield change for climate change for individual model grid cells is -227 t $ha^{-1}$ to 111 t $ha^{-1}$. Large magnitudes of yields are mainly driven by cropland distributions and yields occur most frequently during rainfall on snowpack conditions. Results indicate that impacts on yield change from extreme wildfires are greater than impacts from climate change while climate change has important potential on erosion variability.

TABLE OF CONTENTS

Page

LIST OF TABLES

LIST OF FIGURES

# Dedication

This thesis is dedicated to my beautiful and caring wife.

# CHAPTER ONE

## JOURNAL SUBMISSION

The following chapters will form the majority of an article, which will include my committee members as co-authors, submitted to an open source journal titled Hydrology and Earth System Sciences (HESS). This journal encourages innovative research focusing on what roles water, ecosystems, and humanity have on earth. Submitted journals are peer-reviewed through a discussion journal before revision and final acceptance.

Acknowledgment is required to Jennifer Adam and Mike Barber for their contribution in writing much of Chapter Two as well as parts of the overviews for the modeling framework and models in Chapter Three.

# CHAPTER TWO

# INTRODUCTION

## 2.1 Overview and Objectives

Increasing greenhouse gas concentrations have perturbed the radiative balance of the earth-atmosphere system and led to human-induced global climate change (IPCC 2007). There is strong scientific evidence indicating that climate change is expected to increase the frequency, duration, and intensity of extreme temperature and precipitation events and thus negatively impacting associated heat wave, drought, flood, and wildfire phenomena (CCSP 2008). In the western U.S., there is clear concern for increases in wildfire occurrence and severity due to projected climate changes. For example, the spatial coverage of wildfires in central Idaho during 2001-2010 was 14 times larger compared to the wildfires from 1971-1980 (USACE 2012). Erosion and excess sediment is an important process that affects ecosystems and waterways by adversely impacting aquatic life, navigation, reservoir sedimentation and flood storage, drinking water supply, and aesthetics (Espinosa et al. 1997; Wood and Armitage 1997; Owens et al. 2005; Robertson et al. 2007). The impacts of climate change are expected to increase erosion through disturbances (such as wildfire) developed from changes in temperature and hydrology (Goode et al. 2012).

The overall goal of this study was to quantify the relative roles of (and interactions between) climate change and extreme wildfires in sediment generation due to runoff erosion at larger scales across the PNW. The first objective was to advance the capability to simulate post-fire runoff erosion at scales larger than a single hillslope to examine the relative sensitivity of erosion to wildfire and climate change. This objective was met by implementing and parameterizing a modeling framework that combines models for hillslope-scale erosion (using a representative hillslope

approach) with large-scale hydrology. As a proof of concept for large-scale post-fire erosion modeling, this model was implemented over a large watershed in central Idaho that has been relatively undisturbed by human activities. Following calibration and evaluation, this modeling framework was used to simulate future scenarios to examine the relative sensitivity of SRB erosion rates to wildfire and climate change. The second specific objective for this study was to advance the scientific understanding of the interactions between climate, hydrologic processes, fire severities, and post-fire erosion. These interactions vary across land surface conditions such as vegetation, elevation, slope, and fire burn severity.

## 2.2 Background

### 2.2.1 Wildfire Effects on Erosion

Runoff-induced erosion is important because excess sediment in streams continues to be a concern for resource managers across the United States. Statistics compiled by the U.S. Environmental Protection Agency (EPA) in 1996 and 1998 indicated that 24% of surface water impairment involved sediments, suspended solids, or turbidity (McCutcheon and Pendergast 1999). Uncontaminated suspended and embedded sediments were identified in 15% of 303(d) listed water (Schubauer-Berigan et al. 2005).

The connection between forest fires and erosion has long been established. For example, degradation of water quality occurs in post-fire periods due runoff water erosion of bare soils (Reneau et al. 2010). Also, infiltration rates often are reduced by 50% or more as a result of wildfires (Robichaud 2000; Moody and Martin 2001) leading to increases in overland flow rates. Soils can be directly affected by fire, making them water repellent (Doerr et al. 2006) or reducing their aggregate size (DeBano et al. 2005) and thereby making soils more erodible. Further, the

burning of surface cover results in a loss of protection to soil surface (Benavides-Solorio and MacDonald 2005; Larsen et al. 2009) and leads to greater erosion rates after high severity fires (Connaughton 1935; Benavides-Solorio and MacDonald 2001; Moody and Martin 2001; Holden et al. 2006; Moody and Martin 2009; Robichaud et al. 2010). Comparing burned to non-burned areas, Johansen et al. (2001) found up to 25 times the erosion rate for burned areas. Fire in a 564-ha forested catchment in central Washington produced dramatically increased sediment volumes due to flow rates, increased overland flow caused by reduced infiltration capacity, and mass soil movement (Helvey 1980).

Widespread erosion was reported due to the 1988 Yellowstone fires (Minshall and Brock 1991) and a wildfire in southern Oregon produced 2 to 4 cm of surface soil erosion from steep slopes in a single, intense winter storm (Amaranthus and Trappe 1993). Inbar et al. (1998) used field plots of burnt and undisturbed forests and found sediment yield to be 100,000 times higher in burnt areas the first rainfall season after the fire. This decreased by two orders of magnitude during the second season due to rapid re-vegetation of the area. The increased sediment supply to stream channels often lasts for decades after fires occur (Benda et al. 2003; Moody and Martin 2009). In the Pacific Northwest (PNW), Teasdale and Barber (2008) and other researchers found that forest wildfires likely provide a large percent of the coarser sands that settle in navigation channels and in reservoirs (Elliot et al. 2010; Boll et al. 2011). A recent study on the effects of climate change and wildfire on erosion in central Idaho has suggested that sediment yields could potentially increase by ten-fold from observed long-term rates (Goode et al. 2012).

### 2.2.2 Modeling Erosion

As demonstrated in Section 2.2.1, the effects of wildfire on erosion have been studied and documented for many decades. Likewise, efforts in modeling erosion have resulted in many tools and techniques, both empirically and process-based, that estimate erosion. Beginning in the 1950s, the universal soil loss equation (USLE; Wischmeier and Smith 1978), provided a powerful, empirical tool to estimate erosion (Renard et al. 1991). The USLE computes soil loss by multiplying a series of factors that describe the climate, soil erosivity, topography, land use, and land management (Wischmeier and Smith 1978). Developed initially for farm planning and cropland, the USLE was applied to specific field plots to estimate average annual soil loss. The following decades yielded many updates to the USLE, including the revised universal soil loss equation (RUSLE; Renard et al. 1991), the modified USLE (MUSLE; Williams and Berndt 1977), and RUSLE2 (Lown et al. 2000; Foster et al. 2000). The RUSLE includes updates to each factor based on widespread review and analysis of data from the USLE. The MUSLE uses runoff as the main driver for erosion instead of rainfall. The RUSLE2 model is updated through removal of the requirement for most factors to be applied on average annual basis.

However, these empirical tools are limited when applied to different conditions than for those under which they were developed (Laflen et al. 1991). Thus the need of a more comprehensive and mechanistic erosion model became apparent. Four federal agencies striving to create a new erosion model began work on the Water Erosion Prediction Project (WEPP) model (Laflen et al. 1991). WEPP is a process-based model that includes detachment, transport, and deposition processes (Laflen et al. 1991). This model was the foundation for the erosion calculations in this study.

2.2.3 Study Domain

As mentioned in Section 2.1, the overall goal was to develop the capacity to perform mechanistic erosion simulations over the entire PNW. Within the PNW, the Salmon River basin (SRB) was selected as the study domain. The SRB is largely un-impacted by human uses as compared to the other basins within the PNW. As demonstrated by Figure 1, the basin is primarily forested with some grassland, but with very little cropland or urban areas. The elevation in the SRB ranges from 304-3,713 m. It is one of the largest undeveloped watersheds in the U.S. (~36,000 $km^2$) with 27% of the basin federally protected and nearly 90% owned by the Bureau of Land Management (BLM) and the U.S. Forest Service (USFS) (Tetra Tech 2006).

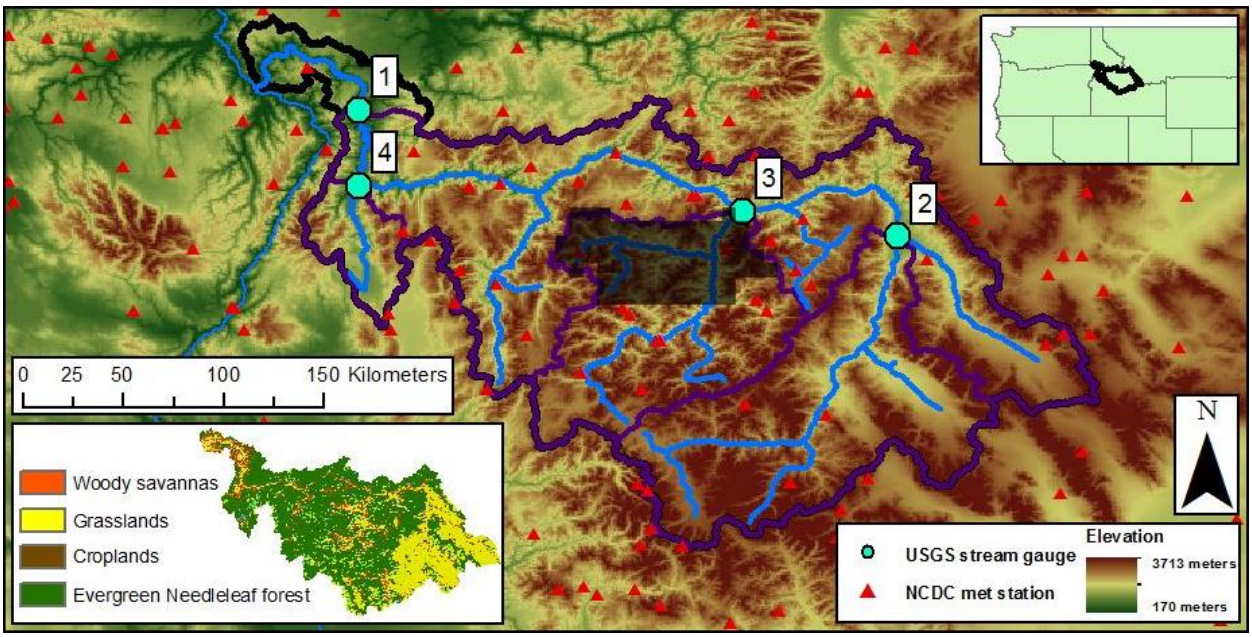


Figure 1. Salmon River basin map showing calibration basins in purple (with basin number reference), elevation, land cover, National Climate Data Center (NCDC) stations, and test area (shaded).

The sediment contributions from the SRB play an important role with respect to flood control, irrigation, infrastructure, and navigation in the Lower Snake River (LSR). For example, a recent Environmental Impact Statement (EIS) by the U.S. Army Corps of Engineers (USACE)

stated that accumulation of sediment could obstruct the function of Lower Granite Project levees (first downstream dam from the SRB) which provides flood protection for the cities of Lewiston and Clarkston (USACE 2012). Suspended sediment measurements from 2008-2011 showed that 53.5% of the total sediment (65.2% of the total sand) entering the Lower Granite Reservoir was generated within the SRB (USACE 2012). A previous report by the USACE stated that 69% of the total sediment contributing to Lower Granite Reservoir originates in the SRB (USACE 2011a) although the SRB only comprises 43% of the LSR basin area. Elliot et al. (2010) stated that the greatest amount of erosion comes from areas affected by wildfire in forested areas. This is significant for the SRB because the majority of the basin is forest and climate change could potentially increase wildfire frequency and severity in forested areas, but the factors driving the interactions between climate change and wildfire are complex (Westerling et al. 2006). The primary source of sediment yield from the SRB comes from disturbed areas, such as forest fires and roads (Goode et al. 2012), with yields ranging from 1 t $ha^{-1}$ to 17.5 t $ha^{-1}$ (Elliot et al. 2010).

Two other modeling studies were performed by Tang et al. (2012) and Sridhar et al. (2012), both of which involved application of the VIC model to examine the sensitivity of SRB streamflow to potential changes in climate. Tang et al. (2012) found that the daily streamflow center of timing shifted to earlier in the season with increased air temperatures of 3 ˚C. Sridhar et al. (2012) found that basin runoff could decrease by 3% as well as shift in peak flow by 10 days from earlier snowmelts. Kunkel and Pierce (2010) reconstructed snowmelt events in the SRB to improve the understanding of climate change on snowmelt-dominated basins. The authors show that recent decades (1985-2007) have earlier reconstructed snowmelt timings compared to previous decades (1940-1980) which they predicted correlates with increases in wildfires. Our study is unique from these other studies in that we considered the relative and interacting effects

of climate change and extreme wildfire events on runoff erosion through large-scale, physically-based model simulations.

Due to the plethora of natural resources in the SRB, parts of the basin have seen significant disturbances such as timber harvesting, grazing, mining, and cropping. Approximately 40% of the Federal land is managed for timber harvest and rangeland. Although these activities have been occurring since the mid-1800s, timber harvest has seen large declines in some areas, mining operations have seen widespread decline, and cropping and grazing activities have seen little change in the last 30 years (Tetra Tech 2006). While timber harvest has disappeared in some areas, the roads from these past activities continue to be a source of sediment in the SRB (Tetra Tech 2006). Although these disturbances are important sources of sediment, the unmanaged lands in the SRB are also susceptible to erosion through natural disturbances, particularly wildfire. During the years of 1971-1980, wildfire affected approximately 500 $km^2$ in the SRB as compared to 7,200 $km^2$ during the time period of 2001-2010 (USACE 2012).

# CHAPTER THREE

# METHODS

## 3.1 Overview of the Modeling Framework

Mao et al. (2010) have recently coupled the Variable Infiltration Capacity (VIC) model to the WEPP-Hillslope Erosion (WEPP-HE) program (Flanagan et al. 2005). WEPP-HE is a stand-alone process-based erosion model that has been extracted from the full WEPP model. There are four groups of information passed to WEPP-HE for simulating runoff erosion at the hillslope scale. First, for each VIC model grid cell, the VIC model passes hydrologic information (runoff depth, peak runoff rate, effective runoff duration, and effective rainfall intensity and duration) to WEPP-HE. Second, downscaled slopes representative hillslopes are randomly selected from each slope gradient and vegetation classification group within a VIC model grid cell. Third, soil information required beyond that needed for VIC modeling includes baseline erodibility, soil particle size classes, size class specific gravity, and organic matter content (Mao et al., 2010). Fourth, erodibility adjustments (due to ground cover, canopy effects, live and dead root biomass, and residue) are handled in the coupled model using a variety of relationships that were developed by Mao et al. (2010). These groups of information are discussed in Section 3.1.3.

### 3.1.1 Variable Infiltration Capacity (VIC) model

The VIC model version 4.1.1 is a fully-distributed, physically-based regional-scale model which solves the water and energy budgets at every time step (from 1-24 hours) and for every grid cell (Liang et al. 1994). It is developed for large-scale applications (1/16 - 2°), in which sub-grid variability in land cover, topography, and saturated extent is based on statistical relationships. The VIC model accounts for key moisture and energy fluxes between the land surface and the atmosphere and includes

algorithms for shallow subsurface (frozen and unfrozen) moisture, snow, lake, and wetland dynamics (Cherkauer and Lettenmaier 1999; Andreadis et al. 2009; Bowling and Lettenmaier 2010). The VIC model has been applied over all continental land areas, and has been used extensively over the western U.S. (e.g., Hamlet and Lettenmaier 1999; Maurer et al. 2002; Elsner et al. 2010; Hamlet et al. 2012) as well as the SRB (Tang et al. 2012; Sridhar et al. 2012).

### 3.1.2 Water Erosion Prediction Project (WEPP) model

The processes represented in WEPP include those for erosion, hydrology, hydraulics, plant growth and residue, water use, and soils (Laflen et al. 1991). The erosion processes in WEPP include detachment (interrill and rill), transport, and deposition. Interrill erosion is the process of raindrops and shallow flows detaching soil particles whereas rill erosion occurs when deeper flowing water detaches soil particles, thus forming rills and gullies. For this study, we excluded channel routing, although WEPP does have this capability. The scale of application for WEPP is typically in the range of a hillslope (tens of meters) to a small watershed (hundreds of meters) (Flanagan and Nearing 1995).

### 3.1.3 Coupling the VIC model and WEPP-HE

We follow the procedures outlined by Mao et al. (2010) to perform rainfall disaggregation, hydrologic input calculation, spatial downscaling of the slope profile, soil characteristic determinations, erodibility adjustment, and hillslope erosion and slope sampling. Each of these procedures is briefly described in Sections 3.1.3.1 – 3.1.3.6. Our contribution to these procedures was for post-fire adjustments within the modeling framework and is presented in Section 3.1.3.7.

#### 3.1.3.1 Rainfall disaggregation

Fine temporal resolution precipitation data to simulate soil erosion are important to reduce the amount of uncertainty in predicting soil loss (Kandel et al. 2004). As most available precipitation data exist on daily time scales, a process was used to disaggregate precipitation data from daily to hourly time scales (Mao et al. 2010). Using monthly precipitation statistics from the National Soil Erosion Research Laboratory (NSERL), rainfall duration, relative time to peak, and relative peak rainfall intensity were produced using CLIGEN, a stochastic weather generator, while maintaining daily precipitation totals (Zhang and Garbrecht 2003; Nicks et al. 1995, Mao et al. 2010). Finally, a WEPP model subroutine called DISAG was used to disaggregate daily precipitation into hourly following a double exponential function while conserving total daily precipitation amounts (Flanagan et al. 1987).

#### 3.1.3.2 Hydrologic Input Calculations

The disaggregated hourly precipitation data were used as the time-variant input to the VIC model (with daily data of maximum and minimum temperature and average wind speed), which was simulated in full water balance mode at hourly time-steps to generate hourly runoff amounts for each grid cell. These meteorological and runoff data were used to generate the following five hydrologic parameters needed for driving WEPP-HE: total runoff depth, peak runoff rate, effective runoff duration, effective rainfall intensity, and the effective rainfall duration. Mao et al. (2010) found that the VIC model predicted more frequent small runoff events that greatly overestimated erosion as compared to the full WEPP model. The small runoff events were related to the VIC model's use of the variable infiltration curve to represent infiltration variability over large spatial areas. By design, the curve assumed that there was

always at least a small fraction of a grid cell that would produce runoff, thus theoretically representing direct rainfall on rivers, wetlands and low lying saturated areas (Mao et al. 2010). These areas do not typically contribute significantly to erosion, so it was determined that erosion estimation should only be calculated when the effective saturation area of the grid cell based on the variable infiltration curve exceeded a minimum threshold (Mao et al. 2010). Based on comparisons to the full version of WEPP, the saturated area threshold was set to 7.5%, so VIC model output was not passed to the WEPP-HE program for soil loss calculations unless the saturation area was greater than that value (Mao et al. 2010).

#### 3.1.3.3 Spatial Downscaling of the Slope Profile

Due to the discrepancy in spatial scales between the VIC model (~5-15 km) and WEPP-HE (~10-100 m), a process was used to downscale digital elevation model (DEM) data to 30 m slopes. Although 30 m DEM data were available for the Mao et al. (2010) study, the authors selected 30 arc second (approximately 1 km) DEM data because they are available globally, easy to manage on large-scales, and commonly used to set up large-scale models, such as the VIC model. Similarly, coarse DEM data were used to determine 30 m rescaled slopes. Mao et al. (2010) applied the VIC-WEPP model at a 1/8° scale and used 30 arc second DEM data, which resulted in 225 elevation pixels within each VIC model grid cell. For this study, the VIC model was applied at a 1/16° resolution and used a 15 arc second (approximately 500 m) DEM. The DEM data were downscaled using a monofractal scaling method to derive 30 m slopes (Bowling et al. 2004).

#### 3.1.3.4 Soil Characteristics

Soil parameters included in the VIC model were based on the State Soil Geographic Data Base (STATSGO) and were gridded to 1/16° resolution with three soil layers. Although soil properties changed from cell to cell, soil properties were constant in each model grid cell. The additional soil inputs required to simulate the WEPP-HE program included baseline erodibility and specific gravity, fraction of sediment, diameter, and fractions of sand, silt, clay, and organic matter in each soil particle size class (Mao et al., 2010). We estimated three baseline erodibility factors for use in WEPP-HE: (1) interrill erodibility which measured the soil rate transfer to rills, (2) rill erodibility which described how vulnerable soil was to detachment by rill flow, and (3) critical shear stress that determined the shear stress at which no erosion occurs (Mao et al. 2010; Elliot et al. 1989; Flanagan and Nearing 1995). After including organic matter in the VIC model soil database, size distributions, fractions, and specific gravities were calculated using a WEPP subroutine (Mao et al. 2010).

#### 3.1.3.5 Erodibility Adjustments

The baseline erodibility factors described in Section 3.1.3.4 were adjusted to account for ground cover, canopy effects, and root biomass which impact the force required to detach soil (Mao et al. 2010). The WEPP-HE erosion model did not include the erodibility adjustment subroutines required to calculate the erodibility adjustments needed as inputs to WEPP-HE, thus Mao et al. (2010) included a subroutine in the VIC-WEPP model process which performs these adjustments. To do this, Mao et al. (2010) developed an interpolation scheme by running the full WEPP model with varying vegetation types to identify seasonal values of erodibility factors for ranges of rainfall amounts and slope gradients. The authors incorporated these seasonal values

for each vegetation type by interpolating between the coupled model's rainfall, slope, and day of year to determine unique erodibility adjustments based on results from the full WEPP model.

3.1.3.6 Hillslope Erosion and Slope Sampling

A sampling scheme based on Park and Van de Giesen (2004) and Thompson et al. (2006) was used to select representative hillslopes within a VIC model grid cell, which reduced computation time but minimized sampling errors (Mao et al. 2010). First, the distribution of representative hillslopes from the downscaled 15 arc second DEM was grouped into similar slope ranges (Table 1). Hillslopes were sampled randomly from each slope range but proportionally based on the number of slopes in each range and the total number of slopes. Each slope range was divided further into different vegetation types according to the fractional area of vegetation in each slope range. This process reduced the number of times WEPP-HE was to be simulated while representing the heterogeneity in slope and vegetation across hillslopes within each VIC model grid cell. Total erosion for each VIC model grid cell was calculated as the sum of the sediment yield from all vegetation and slope groups multiplied by the fractional area of each within the hillslope (for vegetation) and the VIC model grid cell (for slope). Table 1 shows the slope ranges, the number of sampled slopes in each range, the percent of slopes in each range compared to the total number of sampled slopes (166,156), and the average slope in each slope range for the entire SRB.

Table 1. Summary of slope ranges, number of sampled hillslopes for each slope range, percentage of sampled hillslopes to total sampled hillslopes, and the average slope in each slope range in the SRB.

| Slope range, S (%) | Number of sampled hillslopes in slope range | Percentage of sampled hillslopes to total sampled hillslopes in the SRB (%) | Average slope in slope range (%) |
|---|---|---|---|
| < 20 | 37,685 | 22.7 | 11.7 |
| 20 <= S < 36 | 46,140 | 27.8 | 28.1 |
| 36 <= S < 52 | 37,257 | 22.4 | 43.5 |
| 52 <= S < 70 | 24,824 | 14.9 | 60.0 |
| S >= 70 | 20,250 | 12.2 | 89.7 |

3.1.3.7 Post-fire Adjustments

To account for vegetation, soil, and erodibility changes induced by wildfire, adjustment factors for five parameters were calculated: leaf area index (LAI), saturated hydrologic conductivity (Kc), interrill erodibility (Ki), rill erodibility (Kr), and critical shear stress (tc). These five parameters were selected because they were documented as key factors affecting erosion (Parson et al. 2010; Robichaud 2000; Robichaud et al. 2007). LAI adjustment factors for low, moderate, and high fire severity conditions were taken from photographs in Parson et al. (2010). The LAI factor was implemented in the VIC model source code where the vegetation parameters were read (read_vegparam.c). Kc factors for low and high fire severities were developed from Robichaud (2000) with the moderate condition being the average of the low and high fire conditions. These adjustments were implemented in the soil parameter input file for the first soil layer.

The remaining three parameters were adjusted based on WEPP soil database values (Frankenberger et al. 2011) and pre- and post-fire values from Robichaud et al. (2007) for forest

land cover type only because the majority of the SRB is forested. Four soil textures were available in the two sources which included sandy loam, silt loam, clay loam, and loam. From the soil parameter input file, the average VIC model grid cell was composed of 50% sand, 44% silt, and 6% clay. Frankenberger et al. (2011) and Robichaud et al. (2007) specified the soil content for the sandy loam condition as 55% sand, 35% silt, and 10% clay. This condition was the closest composition as compared to that of the average VIC model grid cell and so was selected over the three other soil textures available. Table 2 provides the values for no, low, and high fire severity conditions for Ki, Kr, and tc parameters from Frankenberger et al. (2011) and Robichaud et al. (2007) for the forest sandy loam condition. After averaging the two sources, the adjustment factor was calculated as the quotient of the post- and pre-fire parameter values. For example, the Ki high fire adjustment factor of 2.250 was calculated by dividing 900,000 kg s $m^{-4}$ (high fire value) by 400,000 kg s $m^{-4}$ (no fire value). The moderate fire values were calculated as the average of the low and high conditions. As shown in Table 2, the tc parameter does not change with low and high fire conditions which implies Frankenberger et al. (2011) and Robichaud et al. (2007) did not find tc to change with post-fire, forest conditions. For this study, tc was not included in post-fire adjustments. The Ki and Kr post-fire adjustment factors were applied in the soil adjustment code (adjust_new.f). A summary of the post-fire adjustment factors is listed in Table 3.

Table 2. Initial values for Ki, Kr, and tc for the forest land cover type and sandy loam soil texture. The average parameter value from Frankenberger et al. (2011) and Robichaud et al. (2007) is also provided and is used to calculate the adjustment factors in Table 3.

| Parameter (units) | Severity | Forest Sandy Loam Soil Texture | | Average of two sources |
|---|---|---|---|---|
| | | Elliot and Hall (2010) | Frankenberger et al. (2011) | |
| Ki (kg s $m^{-4}$) | nofire | 400000 | 400000 | 400000 |
| | low | 400000 | 1000000 | 700000 |
| | high | 400000 | 1400000 | 900000 |
| Kr (s $m^{-1}$) | nofire | 0.00050 | 0.00003 | 0.00027 |
| | low | 0.00060 | 0.00040 | 0.00050 |
| | high | 0.00070 | 0.00050 | 0.00060 |
| tc (N $m^{-2}$) | nofire | 1 | 2 | 1.5 |
| | low | 1 | 2 | 1.5 |
| | high | 1 | 2 | 1.5 |

Table 3. Adjustment factors (which were used to rescale the pre-fire parameter values) for key post-fire erosion parameters for no, low, moderate, and high fire severity conditions as implemented in the VIC-WEPP model.

| Parameter | Adjustment factors | | | |
|---|---|---|---|---|
| | No Fire | Low Fire | Moderate Fire | High Fire |
| LAI | 1.000 | 0.600 | 0.250 | 0.050 |
| Kc | 1.000 | 0.900 | 0.775 | 0.650 |
| Ki | 1.000 | 1.750 | 2.000 | 2.250 |
| Kr | 1.000 | 1.887 | 2.075 | 2.264 |
| tc | 1.000 | 1.000 | 1.000 | 1.000 |

## 3.2 Model Calibration and Evaluation

The VIC model was simulated on an hourly time step and aggregated to a daily time step prior to a streamflow routing process (Route 1.0; Lohmann et al. 1996; Lohmann et al. 1998). The resulting hydrographs were compared to U.S. Geologic Survey (USGS) stream gauges at four locations within the SRB. Table 4 provides the basin reference number from Figure 1, the USGS station name, and time periods for calibration and evaluation. Parameters from the soil input file (variable infiltration curve parameter, $b_i$; maximum velocity of baseflow, Dsmax (mm $day^{-1}$); fraction of maximum velocity of baseflow where non-linear baseflow begins, Ds; fraction of maximum soil moisture where non-linear baseflow occurs, Ws; second soil layer, $D_2$ (m); third soil layer, $D_3$ (m); and snow surface roughness, Snow_rough (m)) were adjusted according to the VIC model technical documentation with $D_2$ (maximum value increased to 5.5 m from 1.5 m) and Snow_rough (maximum value increased to 0.6 m from 0.2 m) parameters' ranges expanded to match the shape of the hydrographs (Gao et al. 2010). Table 5 shows the initial ranges of the calibration parameters from Gao et al. (2010) and the values used in this study.

Table 4. USGS station names and time periods for each basin for calibration and evaluation.

| Basin | Station Name | Period of Calibration | Period of Evalution |
|---|---|---|---|
| | | (mmm yyyy - mmm yyyy) | |
| 1 | SALMON RIVER AT WHITE BIRD ID | Jan 1979 - Dec 1994 | Jan 1995 - Dec 2010 |
| 2 | SALMON RIVER AT SALMON ID | Jan 1979 - Dec 1994 | Jan 1995 - Dec 2010 |
| 3 | MF SALMON RIVER AT MOUTH NR SHOUP ID | Oct 1993 - Mar 2002 | Apr 2002 - Sep 2010 |
| 4 | LITTLE SALMON RIVER AT RIGGINS ID | Jan 1979 - Dec 1994 | Jan 1995 - Dec 2010 |

Initial incoming shortwave radiation was empirically estimated in the VIC model so was available for adjustment and were used to adjust the timing of peak flow for simulated flows. Incoming shortwave radiation was adjusted by fractions after it was calculated (initialize_atmos.c). In a study in Colorado, VIC model simulated streamflow was calibrated and evaluated with success using incoming radiation as well as other parameters (Barsugli et al. 2012). Solar radiation and the amount of radiation reflected from the snow surface are key factors for influencing the timing of snowmelt (Barsugli et al. 2012).

Table 5. Ranges for calibration parameters used in the VIC model calibration with final calibration values for all basins.

| Parameter | Range of Initial Values from Gao et al. (2010) | Range of Values Used | Basin 1 | Basin 2 | Basin 3 | Basin 4 |
|---|---|---|---|---|---|---|
| $b_i$ | 0.00001 – 0.4 | 0.00001 – 0.4 | Initial | Initial | Initial | 0.4 |
| Dsmax (mm day$^{-1}$) | 0.00001 – 30 | 0.00001 – 30 | Initial | Initial | Initial | Initial |
| Ds | 0.00001 – 1 | 0.00001 – 1 | Initial | Initial | Initial | Initial |
| Ws | 0.00001 – 1 | 0.00001 – 1 | Initial | Initial | Initial | Initial |
| $D_2$ (m) | 0.1 – 1.5 | 0.1 – 5.5 | Initial | 5.5 | 1.5 | Initial |
| $D_3$ (m) | 0.1 – 1.5 | 0.1 – 1.5 | Initial | Initial | 1.5 | 1.5 |
| Snow_rough (m) | 0.005 – 0.2 | 0.005 – 0.6 | Initial | 0.15 | 0.6 | 0.11 |
| Incoming shortwave radiation (adjustment factor) | None | 0.7 – 1.3 | 1.0 | 0.2 | 0.2 | 0.5 |

Each basin was calibrated separately and Table 5 shows the ranges of the individual basin values for parameters calibrated. The parameters with an "Initial" value represent parameters that were not calibrated in this study and follow the default values of Hamlet et al. (2012) as discussed in Section 3.4. A value of 1.0 for incoming shortwave radiation represents basins that did not use this parameter in calibration. Since the three smaller basins were included in Basin One, they were calibrated first which allowed Basin One to be calibrated using the final hydrographs of the smaller basins. For this study, the

initial parameters for Basin One provided sufficient hydrographs so no calibration was necessary for Basin One. Basin Two used a $D_2$ value of 5.5 m, a Snow_rough value of 0.15, and an adjustment factor of 0.2 for incoming shortwave radiation. Basin Three used a $D_2$ and $D_3$ value of 1.5 m, a Snow_rough value of 0.6, and an adjustment factor of 0.2 for incoming shortwave radiation. Last, Basin Four used a $b_i$ value of 0.4, a $D_3$ value of 1.5 m, a Snow_rough value of 0.11, and an adjustment factor of 0.5 for incoming shortwave radiation. Although recent timber harvest and wildfire disturbances have occurred in the SRB (discussed in Section 2.2.3), these disturbances were not accounted for in calibration and evaluation with the simulated historical streamflow using the no fire condition.

Along with matching the shape of the average monthly hydrograph, the Nash-Sutcliffe efficiency (E) (see Equation 1) metric was used to compare the USGS observed and simulated flows (calculated for both daily and monthly time-scales) flows. For each basin, the observed streamflow period of observations was divided into two time periods in which the first half is used for model calibration and the second half for model evaluation (Table 4). For a perfect model, E would have a value of one; if E was less than zero, the observed mean was a better predictor of streamflow than the model. Equation 1 shows the calculation of E where $O_i$ is the observed flow at time *i*, $P_i$ is the simulated flow at time *i*, and $\overline{O}$ is the observed mean flow. Moriasi et al. (2007) performed a review of models using E as the model performance metric and reported typical values of E greater than 0.60 for daily time-steps.

$$E = 1 - \frac{\sum_{i=1}^{n}(O_i - P_i)^2}{\sum_{i=1}^{n}\left(O_i - \overline{O}\right)^2} \quad (1)$$

For the evaluation period, the following additional metrics were calculated: a daily peak flow (PK) metric, averaged yearly relative bias (RB), and daily and monthly root-mean-square

error (RMSE). The peak flow metric was an extreme event creating metric developed by Coulibaly et al. (2001) and applied in this study to check the simulated peak events. A perfect model would result in a peak flow metric of zero. The authors stated that typical values range from 0.1 to 0.15 for a well predicting model. The peak metric was calculated as shown in Equation 2 where $n_p$ is the number of peak flows greater than one-third of the observed mean peak flow, $Q_{pi}$ is the daily observed flow, and $\hat{Q}_{pi}$ is the daily simulated flow (Coulibaly et al. 2001). The authors stated that the PK metric captures extreme events more effectively than the E and RMSE metrics.

$$PK = \frac{\left[\sum_{i=1}^{np}\left(Q_{pi}-\hat{Q}_{pi}\right)^2\left(Q_{pi}\right)^2\right]^{\frac{1}{4}}}{\left(\sum_{i=1}^{np}\left(Q_{pi}\right)^2\right)^{\frac{1}{2}}} \quad (2)$$

$$RB = \frac{\sum_{i=1}^{ny}(P_i-O_i)/(O_i)}{ny} \quad (3)$$

$$RMSE = \sqrt{\frac{\sum_{i=1}^{nm}(P_i-O_i)^2}{n_m}} \quad (4)$$

Equation 3 shows the calculation to determine RB on a yearly time step where $n_y$ is the number of years, $P_i$ is the average annual simulated flow, and $O_i$ is the average annual observed flow. The RMSE was calculated as shown in Equation 4 where $n_m$ is the number of months or days, $P_i$ is the simulated flow, and $O_i$ is the observed flow.

Along with streamflow evaluation, the VIC-WEPP model output was compared to short- and long-term sediment yields from seven locations (32 locations total in Idaho) that fall within the

VIC-WEPP model boundary of the SRB (Kirchner et al. 2001). Kirchner et al. (2001) compiled observed (short-term; record lengths of 10-28 years) sediment yield results from measurements of trapped sediment behind small dams and calculated from daily measurements of streamflow. The authors also measured long-term (time-scales of 6,300-26,000 years) erosion rates from concentrations of cosmogenic radionuclides that determined when sediment was eroded (Kirchner et al. 2001). Since slope and land cover type were not specified for the specific location of samples in Kirchner et al. (2001), the VIC-WEPP model sediment yields that were compared were from the model grid cell that the Kirchner et al. (2001) locations fell within. Although the spatial scales of the model grid cell and the point locations from Kirchner et al. (2001) were different and only seven locations are available in the SRB from the authors, an evaluation provided the general order of magnitude difference between the VIC-WEPP model and observed short-term yields as well as predicted long-term yields.

### 3.3 Model Inter-comparison

A model inter-comparison was performed between the VIC-WEPP model and Disturbed WEPP to explore the extent to which the models agree, including determining whether or not the models predicted values within one to two orders of magnitude of each other, which would be consistent with other studies. For example, a study from the International Geosphere-Biosphere Programme-Global Change and Terrestrial Ecosystems (IGBP‑GCTE) Soil Erosion Network compared four erosion models (including WEPP) which showed simulated soil loss rates within one order of magnitude of observed rates (Jetten 1999). Spigel and Robichaud (2007) showed simulated erosion rates from individual hillslopes within two orders of magnitude of observed rates for hillslopes less than 1 t $ha^{-1}$ and within one order of magnitude for hillslopes greater than 1 t $ha^{-1}$. When hillslope rates were averaged over a large area, all rates were within one order of magnitude (Spigel and Robichaud 2007).

Disturbed WEPP is one of the many online suites of the WEPP model developed by the USFS to allow for easy user use (Elliot and Hall 2010). Users are able to select parameters to produce average annual yields from one hillslope. Using historical climate statistics and the CLIGEN weather generator, daily climate is generated which is then used to estimate erosion. The online user interface is simple and allows the user 15 inputs to select from making this model advantageous for simple applications while maintaining quality in the results.

### 3.3.1 Hillslope Comparison

Disturbed WEPP uses climate, soil texture, topography, vegetation type, and ground cover percent to simulate average annual yields from hillslopes and is designed for forests, rangelands, wildfires, and conditions with little disturbance such as no-till agriculture (Elliot and Hall 2010). For this study, a spreadsheet-based, batch version of Disturbed WEPP was used which enabled multiple hillslopes to be simulated in series which reduces computational time as compared to the single, hillslope version. From the VIC-WEPP model setup, ten grid cells (located in the western half of the SRB) were selected from within the study domain. Each grid cell ranged from 96 to 199 sampled hillslopes and all hillslopes were overlaid with no fire and high fire severity conditions resulting in two scenarios for each model. Low and moderate burn severities were not considered in the model comparison because Disturbed WEPP did not have treatment types for these two conditions.

The same climate, slope, and soil texture as well as similar vegetation type and percent cover data were used in both models. Table 6 compares the main model components for each model. The climate data used in Disturbed WEPP come from the rainfall disaggregation process (see Section 3.1.3.1). The daily storm patterns calculated from CLIGEN are the same for both

the VIC-WEPP model and Disturbed WEPP applications but how the sub-daily inputs were produced and used varies for each model. In the VIC-WEPP model application, the daily storm patterns were processed into hourly rainfall amounts and used in the VIC model hourly simulations. For Disturbed WEPP, the daily input was processed into break point rainfall amounts which define a curve representing the sub-daily rainfall distribution based on intensity rather than time. The sub-daily rainfall amounts were then processed differently by each model to produce runoff which was the main driver in erosion.

Table 6. Comparison of key components of the VIC-WEPP model and Disturbed WEPP.

| Key Model Component | VIC-WEPP | Disturbed WEPP |
|---|---|---|
| Climate Input | Daily data for date, precipitation, precipitation duration, ratio of time to rainfall peak and duration, ratio of maximum rainfall intensity to average rainfall intensity, maximum temperature, minimum temperature, solar radiation, wind velocity, wind direction, and dew point temperature | |
| Soil Texture Input | Uses fractions of clay, silt, and sand | Has four options: clay loam, silt loam, sandy loam, or loam. |
| Treatment/Vegetation Type or Land Cover | Forest, wooded grassland, prairie, cropland, and bare soil | Mature forest, Thin or young forest, Shrubs, Good grass, Poor grass, Low severity fire, High severity fire, Skid trail |
| Erodibility Adjustments | Subroutines based off of full WEPP code with seasonal adjustments by Mao et al. (2010) | Uses full WEPP routines to calcualte adjustments |
| Physical Properties | Slope, slope length | |
| | Width is 3.7 meters | Width is 100 meters |
| Post-processing Output | Average annual sediment yield normalized by area | |
| WEPP Version | v2004.7 | v2010.1 |

Slope and horizontal hillslope length (default value in the VIC-WEPP model is 22.3 m) were the same for both models. Slope length (calculated from the slope and horizontal hillslope length) was the same for the two models. Although the default width in the VIC-WEPP model is

3.7 m and 100 m in Disturbed WEPP, the post-processing of the output for both models normalized the mass yielded by area. Soil textures in Disturbed WEPP could be clay loam, silt loam, sandy loam, or loam and were determined from the VIC-WEPP model (see Section 3.1.3.4) as the largest fraction of clay, silt, and sand (Mao et al. 2010). The vegetation types in the two models were different and are shown in Table 6. The percent cover describes the fraction of soil that had ground cover vegetation. In Disturbed WEPP, rock fragments in the soil altered the flow of water and reduced the hydraulic conductivity (i.e. a 30% rock input reduced hydraulic conductivity by 30%). Default values for % cover and % rock were changed to better describe site-specific conditions as recommended in Disturbed WEPP documentation (Elliot and Hall 2010). Table 7 shows estimations of % cover and % rock for all Disturbed WEPP vegetation to describe the corresponding VIC-WEPP model vegetation type.

Table 7. Vegetation, percent cover, and percent rock inputs used in Disturbed WEPP to represent standard land use types from the VIC-WEPP model.

| VIC-WEPP Vegetation | Disturbed WEPP Vegetation | Disturbed WEPP % Cover | Disturbed WEPP % Rock |
|---|---|---|---|
| Forest | 5 Year Old Forest | 100 | 20 |
| Wooded Grassland | Tall Grass | 80 | 20 |
| Prairie | Short Grass | 50 | 20 |
| Cropland | Tall Grass | 40 | 20 |
| Any type | High Severity Fire | 1 | 40 |

The versions of WEPP in each model were different as the VIC-WEPP model used v2004.7 and as Disturbed WEPP used v2010.1. According to the U.S. Department of Agriculture (USDA) NSERL release notes from updated versions of WEPP, there were two additional versions between the two listed above; v2006.5 and 2008.907 (USDA 2012). The major changes

that occurred in WEPP between v2004.7 and v2010.1 that may affect results between the two models are shown is Table 8 (USDA 2012).

Table 8. List of major changes for three updates to the WEPP model possibly causing differences in the two models (USDA 2012).

| WEPP versions | Changes |
|---|---|
| 2004.7 to 2006.5 | ● Subsurface lateral flow added<br>● Rock correction factor update<br>● Minimum saturated hydraulic conductivity decreased to 0.000000108 mm/hr from 0.07 mm/hr<br>● Radiation inclinations for each overland flow element are calculated separately to more accurately describe snow melt |
| 2006.5 to 2008.907 | ● Winter hydrology subroutines including solar radiation on sloped surfaces, cloud cover estimation, start time of storm<br>● Number of fine layers used in frost simulation added |
| 2008.907 to 2010.1 | ● Watershed runoff possibly larger than precipitation fixed<br>● Soil water content possibly larger than soil porosity fixed<br>● Soil thermal conductivity adjustment updated<br>● Water balance issues fixed<br>● Freeze/thaw energy calculations fixed<br>● Rainfall on snowpack updated<br>● Chezy depth-discharge coefficient calculation fixed<br>● Sediment yield in multiple overland flow elements fixed |

### 3.3.2 Hillslope Sensitivity

Along with a hillslope comparison, sensitivity analysis was done to better understand the factors that caused the most change in each model. Due to the inability to isolate and adjust specific parameters in Disturbed WEPP (because of its web-based nature), two different approaches were performed, one for each model. For Disturbed WEPP, there were four soil textures and eight treatment or vegetation conditions to select from that determined the values for key parameters that affect erosion (Ki, Kr, tc, and effective hydraulic conductivity). The slope,

slope length, and cover inputs were varied with constant soil texture and treatment types to check the influence each of these variables had on sediment yield. The climate input was another factor tested for sensitivity in Disturbed WEPP. To check the impact climate had on erosion estimates in Disturbed WEPP, soil texture, treatment type, slope, and cover inputs were all kept constant while changes were made solely to the climate input.

As the source code of the VIC-WEPP model could be accessed, specific variables were isolated in erosion calculations to show the impacts of a specific variable on erosion. Nine parameters were adjusted in the VIC-WEPP model sensitivity analysis; they included Ki, Kr, tc, Kc, slope, slope length, LAI, land cover type, and climate. Ki, Kr, and tc had ranges of values similar to the same parameters in the Disturbed WEPP sensitivity which were 400,000-1,500,000 kg s $m^{-4}$, 0.0002-0.0007 s $m^{-1}$, and 0.5-1 N $m^{-2}$ for Ki, Kr, and tc, respectively. Kc ranged from 300-2700 mm $day^{-1}$ which was consistent with the range of this variable in the VIC model soil database. For slope, twelve different values were selected with non-linear steps ranging from 0.1 to 110 percent. Slope length was changed from 5 m to 95 m with 5 m steps. LAI was adjusted by factors similar to the way post-fire adjustments were made in Section 3.1.3.7 with a range of 0.4-1.6. Land cover included the five main types used in the VIC-WEPP model: forest, wooded grassland, prairie, cropland, and bare soil. Finally, different locations were used to show the impact of climate on erosion. To reduce uncertainty, the soil parameters, vegetation parameters, and snow band elevation distributions were all exactly the same for each of the ten VIC model grid cells resulting in climate (precipitation, temperature, and wind speed) being the only changing factor between the locations. Table 9 provides a summary of the variables adjusted in the VIC-WEPP model sensitivity test.

Table 9. Summary of VIC-WEPP model and Disturbed WEPP parameters and range of values used in sensitivity analysis.

| Parameter | Range of Values | |
|---|---|---|
| | Disturbed WEPP | VIC-WEPP |
| Interrill erodibility (kg s $m^{-4}$) | 400,000-1,500,000 | 400,000-1,500,000 |
| Rill erodibility (s $m^{-1}$) | 0.0002-0.0007 | 0.0002-0.0007 |
| Critical shear (N $m^{-2}$) | 0.5-1 | 0.5-1 |
| Hydraulic conductivity (mm $day^{-1}$) | 144-1008 | 300-2700 |
| Slope (%) | 1-100 | 0.1-110 |
| Slope length (m) | 5-95 | 5-95 |
| Treatment/Vegetation type or land cover | Mature forest, Thin or young forest, Shrubs, Good grass, Poor grass, Low severity fire, High severity fire, Skid trail | Forest, wooded grassland, prairie, cropland, and bare soil |
| Location - average annual precipitation (mm) | 598-1296 | 598-1296 |
| Cover (%) | 0-100 | -[a] |
| LAI (factor) | - | 0.4-1.6 |

[a] – indicates the parameter was not used in the specific model sensitivity test.

## 3.4 Data Sources

Historical model simulations were driven by gridded daily precipitation, air temperature, and wind speed from Abatzoglou (2011) who used the North American Land Data Assimilation System Phase 2 (NLDAS-2, Mitchell et al. 2004) and the Parameter-elevation Regressions on Independent Slopes Model (PRISM, Daly et al. 2008) to create a high-resolution, 4-km gridded dataset from 1979 to 2010. This dataset was aggregated to the VIC model's 1/16° scale. For future

climate, daily Coupled Model Intercomparison Project Phase 5 (CMIP5) downscaled data, using the Multivariate Adapted Constructed Analogs (MACA) method by Abatzoglou and Brown (2011), from 2039 to 2070 was used. The future model simulations were bias corrected to adhere to the statistics of the observational record (1979-2010). This method was particularly valuable for this project because authors show that MACA is well-suited for ecological sensitive applications which can include ecosystems that would be negatively impacted by large fluctuations of erosion because it conserves the relationships between meteorological variables such as precipitation and temperature (Abatzoglou and Brown 2011). Abatzoglou and Brown (2011) conclude that MACA's approach to treat variables dependently and the ability to track fire danger indices makes this downscaling method advantageous.

The soil and vegetation parameters originated from the Matheussen et al. (2000) 1/8$^{th}$ degree VIC model implementation which was later used to create the 1/16$^{th}$ VIC model parameters for Elsner et al. (2010). This study used the datasets from Hamlet et al. (2012) which provided additional calibration on the Elsner et al. (2010) soil land vegetation parameters. Soil parameters were originally derived from the State Soil Geographic (STATSGO) Data Base (USDA 1994; Nijssen et al 1997, and Kirschbaum and Lettenmaier 1997). Vegetation parameters were originally estimated from the Advanced Very High Resolution Radiometer (AVHRR) satellite data (Loveland et al. 1991; Loveland and Ohlen 1993; Quigley and Arbelide 1997) which were then converted to grid-based maps at 1 km resolution (Menakis et al. 1996; Hann et al. 1997). The land cover used was reclassified from MODIS MOD 12Q1 data with 500-meter resolution (Friedl et al. 2002). Digital elevation model (DEM) data at 500 meters were used from the Global Multi-resolution Terrain Elevation Data 2010 (GMTED2010; Danielson and Gesch 2011).

## 3.5 Model Application

As a final step, the calibrated VIC-WEPP model was applied over the SRB. Five future climate simulations were simulated to examine the sensitivity of the VIC model simulated streamflow to climate in the SRB. The same set of future scenarios was applied to the VIC-WEPP model over a smaller test area (see Figure 1) to quantify additional impacts of climate change on erosion. The test area was determined by selecting an area that included ranges of annual precipitation, average slope, and land cover. For this project, RCP4.5 and RCP8.5 were used which are associated with approximately 4.5 W $m^{-2}$ (approximately 650 ppm $CO_2$-equivalent) and greater than 8.5 W $m^{-2}$ (great than 1,370 ppm $CO_2$-equivalent) of additional energy by the year 2100, respectively (Moss et al. 2010). These RCPs (and others; RCP2.6 and RCP6.0) were identified by the research community based on peer-reviewed literature that describes possible pathways to reach the trajected radiative forcings and concentrations (Moss et al. 2010). As proof of the capability to model erosion at large-scales, historical climate and one future scenario (the MIROC5 model with the RCP4.5 scenario) were used over the entire SRB. Plotting the difference in precipitation and temperature for 24 future scenarios in the SRB, the most extreme (corners) and the center scenarios were used as the five scenarios. Figure 2 shows the range of future scenarios and the selection of the five future scenarios. Table 10 gives a summary of the five models used including the country of origin for each model.

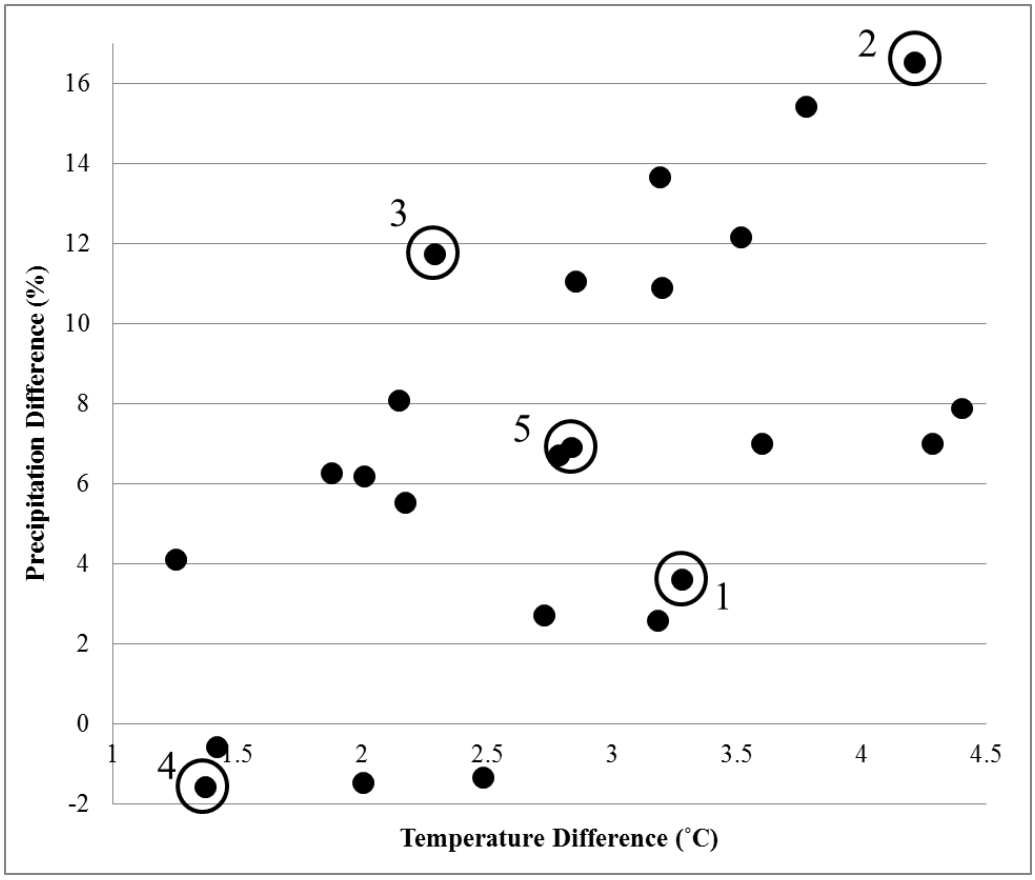


Figure 2. Selection of the five future scenarios was based on the extreme scenarios and middle scenario. Circled points refer to the future scenarios in Table 10.

Table 10. Summary of the five models and scenarios selected for future simulations. Model # refers to the numbers in Figure 2.

| Model # | Modelling group, country | CMIP5 model I.D. |
|---|---|---|
| 1 | Beijing Climate Center, China Meteorological Administration, China | BCC_CSM1.1 RCP8.5 |
| 2 | Canadian Centre for Climate Modelling and Analysis, Canada | CanESM2 RCP8.5 |
| 3 | US Dept. of Commerce/NOAA/Geophysical Fluid Dynamics Laboratory, USA | GFDL-ESM2G RCP8.5 |
| 4 | Institute for Numerical Mathematics, Russia | INMCM4.0 RCP4.5 |
| 5 | Atmosphere and Ocean Research Institute (The University of Tokyo), National Institute for Environmental Studies, and Japan Agency for Marine-Earth Science and Technology, Japan | MIROC5 RCP4.5 |

Figure 3 and Figure 4 show the climate change differences (2039-2070) compared to the long-term, historical (1979-2010), basin-wide average for precipitation and temperature, respectively, on a VIC model grid cell basis. The maps in Figure 3 show the precipitation differences for the BCC_CSM1.1 RCP8.5 (a), CanESM2 RCP8.5 (b), GFDL-ESM2G RCP8.5 (c), INMCM4.0 RCP4.5 (d), and MIROC5 RCP4.5 (e) future scenarios. The five maps in Figure 4 follow the same outline as Figure 3 expect for temperature difference. The precipitation difference was calculated according to Equation 5 with $P_{annual}$ being the VIC model grid cell average annual precipitation for the scenario (historical and future climates) and $P_{hist}$ being the long-term, historical, basin-wide average precipitation which was 726 mm. The temperature difference was calculated according to Equation 6 with $T_{annual}$ being the VIC model grid cell average annual temperature for the scenario (historical and future climates) and $T_{hist}$ being the long-term, historical, basin-wide average temperature which was 3.68 ˚C.

$$Precipitation\ Difference = \frac{P_{annual} - P_{hist}}{P_{hist}} \quad (5)$$

$$Temperature\ Difference = T_{annual} - T_{hist} \quad (6)$$

The basin average precipitation and temperature differences for the BCC_CSM1.1 RCP8.5 scenario in Figure 3(a) and Figure 4(b), respectively, correspond to point one in Figure 2. Similarly, the basin average precipitation and temperature differences for the remaining four scenarios can be found. The majority of precipitation increase is predicted to be located in the center of the SRB where there is mainly forest land cover (Figure 3). The temperature is projected to increase in the majority of the SRB with greatest increases occurring in lower elevations with some decreases in temperature mainly occurring in the INMCM4.0 RCP4.5 scenario and at higher elevations (Figure 4).

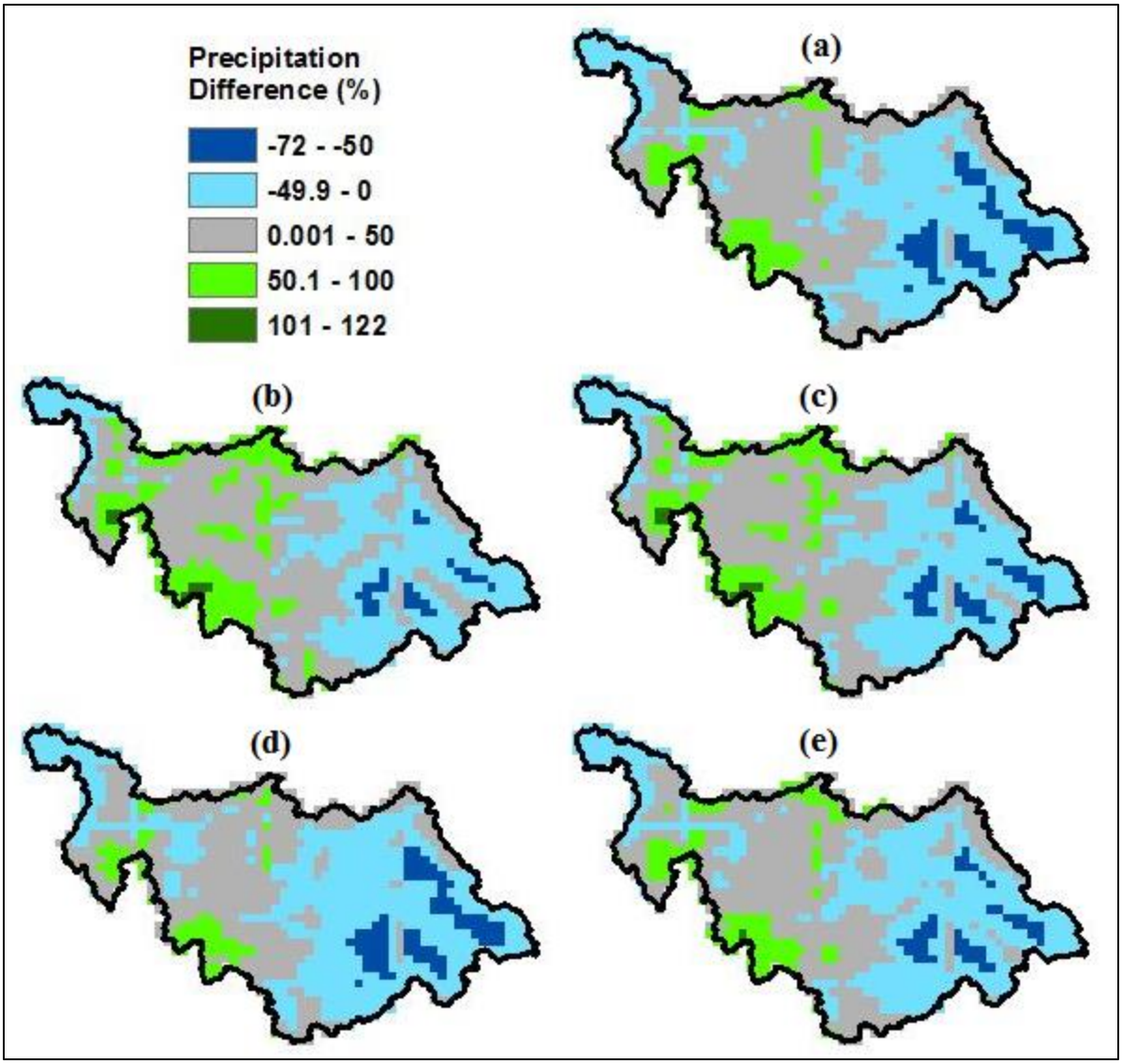


Figure 3. Precipitation differences compared to the long-term historical (1979-2010) precipitation average. Maps (a), (b), (c), (d), and (e), show the precipitation difference for the BCC_CSM1.1 RCP8.5, CanESM2 RCP8.5, GFDL-ESM2G RCP8.5, INMCM4.0 RCP4.5, and MIROC5 RCP4.5 future scenarios, respectively, as calculated in Equation 5.

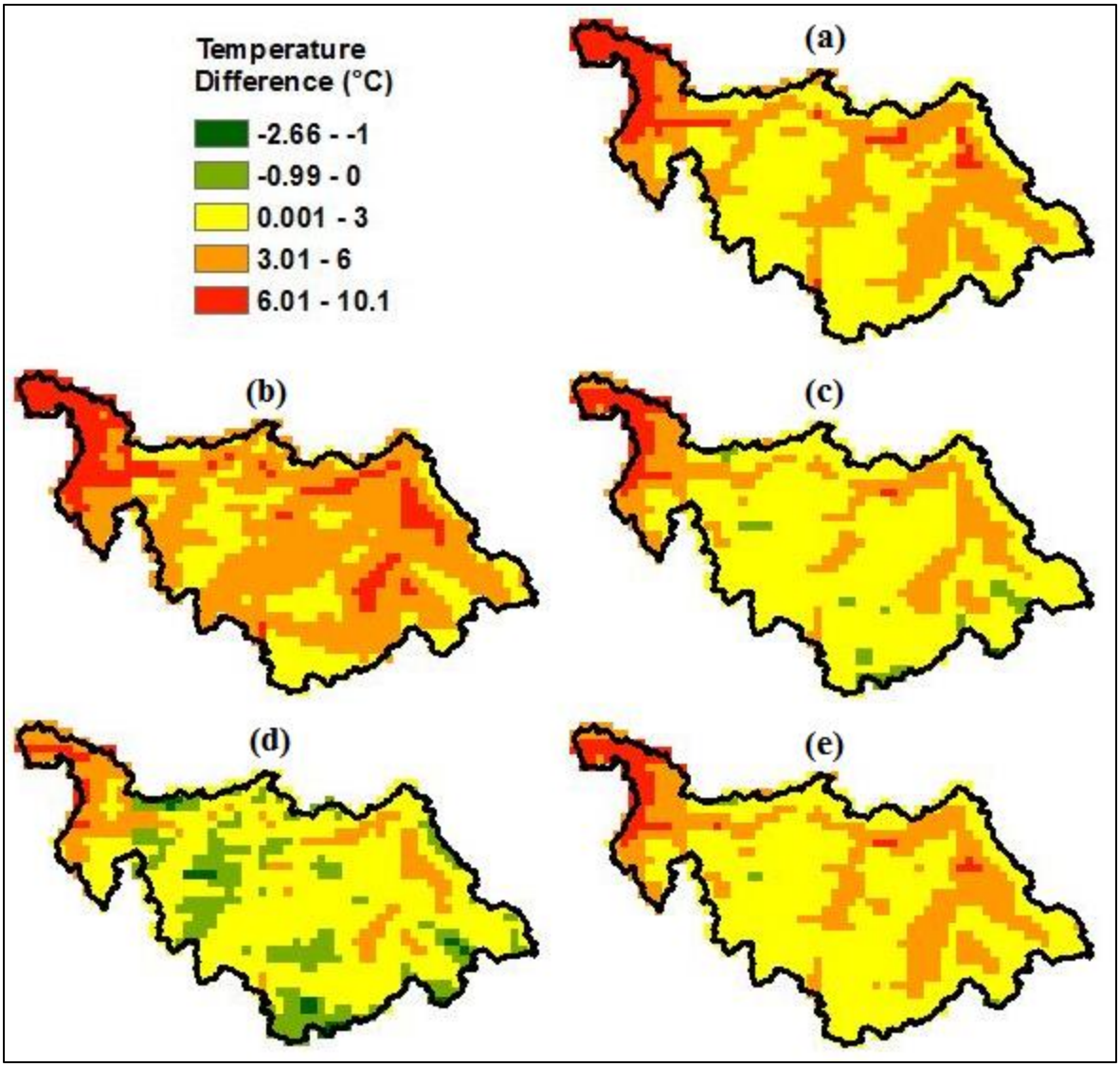


Figure 4. Temperature differences compared to the long-term historical (1979-2010) temperature average. Maps (a), (b), (c), (d), and (e), show the temperature difference for the BCC_CSM1.1 RCP8.5, CanESM2 RCP8.5, GFDL-ESM2G RCP8.5, INMCM4.0 RCP4.5, and MIROC5 RCP4.5 future scenarios, respectively, as calculated in Equation 6.

# CHAPTER FOUR

# RESULTS AND DISCUSSIONS

## 4.1 Model Calibration and Evaluation

Simulated historical streamflow at four basins (see Figure 1) within the SRB were compared to USGS observed records for calibration and evaluation time periods. The historical simulations only considered the no fire condition and graphs of average Julian day, average monthly, and daily flows are only shown in this chapter for Basin One with all other basins' graphs shown in the Appendix.

Model performance was shown visually and by metrics. Table 11 and Table 12 show the metrics results for each basin for calibration and evaluation, respectively. For the calibration time period, the largest basin had E values of 0.88 and 0.96 for daily and monthly time steps, respectively. During evaluation, the same basin had E values of 0.83 and 0.93 similarly for daily and monthly time steps. As with Basin One, Basin Four had E values that declined for both daily and monthly time steps when comparing the calibration period to the evaluation period. Basin s two and three had E values that increased during the evaluation period for both daily and monthly time steps. Streamflow results for all basins except Basin Two had E values greater than 0.60 for the calibration and evaluation time periods. Tang et al. (2012) had monthly calibrated E values of 0.81 and 0.82 for Basin One and Basin Two, respectively, which were less than the monthly calibrated E values in this study.

The PK values for all basins were within the well predicted values from Coulibaly et al. (2001) showing these basins capture peak flows relatively well. The RMSE daily and monthly values are scale dependent and therefore increased when the streamflow values increased. The RMSE values in Table 12 show the errors associated with simulated streamflow. Basin Three had the best result of yearly RB at -0.003 and all basins showing yearly RB within ±15% bias.

Table 11. Calibration E metrics for all basins as well as basin area, percent of total area, and percent of total streamflow.

| Basin | E | | Basin Area ($km^2$) | Percentage of Total Calibration Area | Percentage of Total Streamflow |
|---|---|---|---|---|---|
| | Daily | Monthly | | | |
| 1 | 0.88 | 0.96 | 34760 | 100% | 100% |
| 2 | 0.41 | 0.56 | 9679 | 27.8% | 15.0% |
| 3 | 0.60 | 0.83 | 7449 | 21.4% | 28.0% |
| 4 | 0.76 | 0.93 | 1491 | 4.3% | 7.0% |

Table 12. Evaluation metrics for all basins.

| Basin | E | | PK | RMSE ($m^3 s^{-1}$) | | RB |
|---|---|---|---|---|---|---|
| | Daily | Monthly | | Daily | Monthly | |
| 1 | 0.83 | 0.93 | 0.095 | 162 | 884 | -0.098 |
| 2 | 0.59 | 0.81 | 0.108 | 34.6 | 187 | 0.148 |
| 3 | 0.71 | 0.90 | 0.124 | 52.5 | 279 | -0.003 |
| 4 | 0.75 | 0.88 | 0.099 | 14.0 | 75.1 | -0.103 |

Hydrographs are only shown in this chapter for Basin One with all other basins' shown in the Appendix. Figure 5 shows the observed and calibrated simulated discharge at the outlet of Basin One for (a) the average Julian day, (b) average month, and (c) three years of daily flows. The average Julian day hydrographs are shown to give additional detail to the average monthly hydrographs and the daily flows provide hydrographs for non-averaged flows. Figure 6 has similar graphs as Figure 5 but for the evaluation period. The simulated flow in Figure 5(b) shows a one month earlier peak than observed flow. The evaluation comparison in Figure 6 also follows similar patterns.

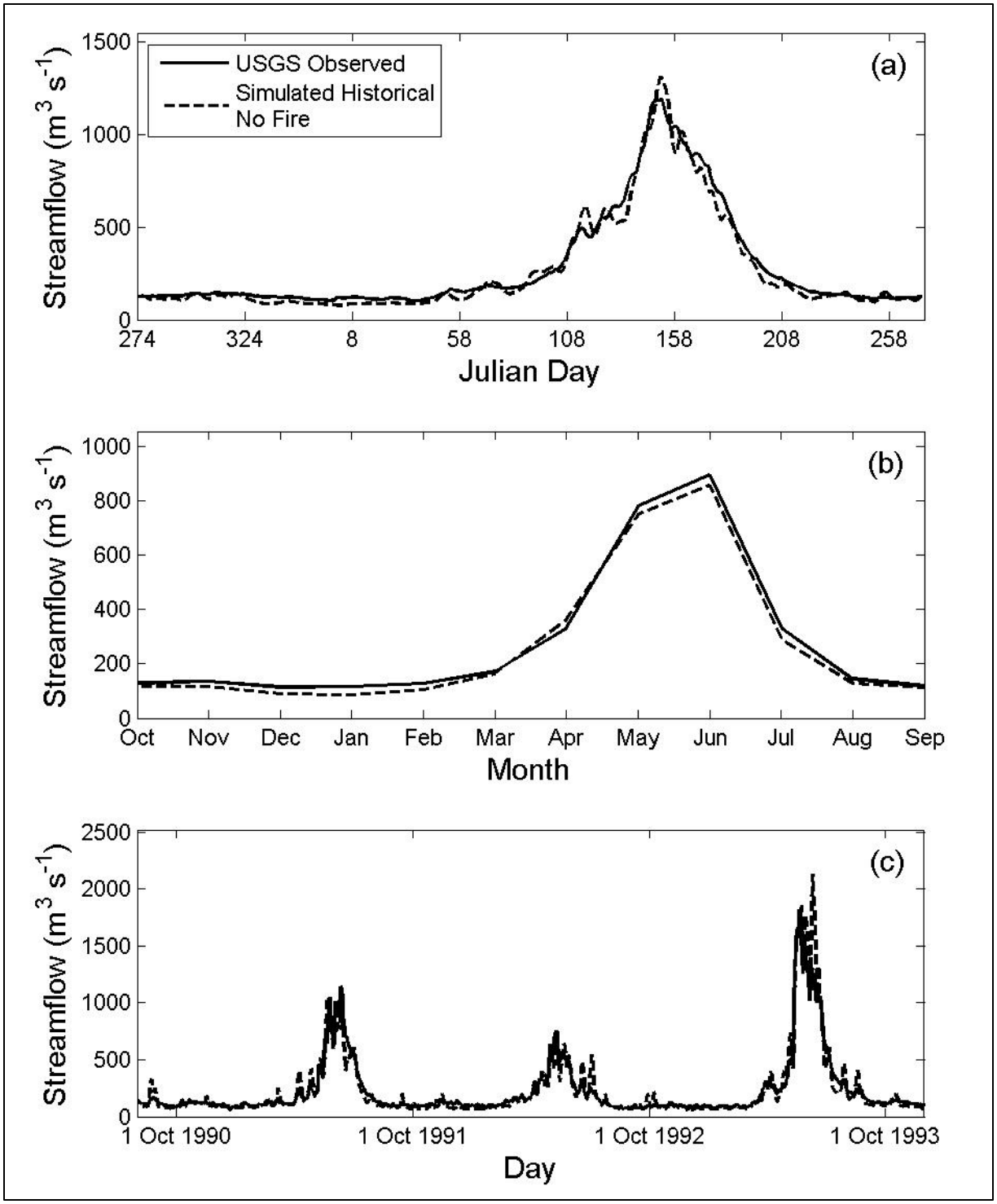


Figure 5. Observed and simulated discharge for the calibration period at the outlet of Basin One for (a) the average Julian day, (b) average month, and (c) three years of daily flows.

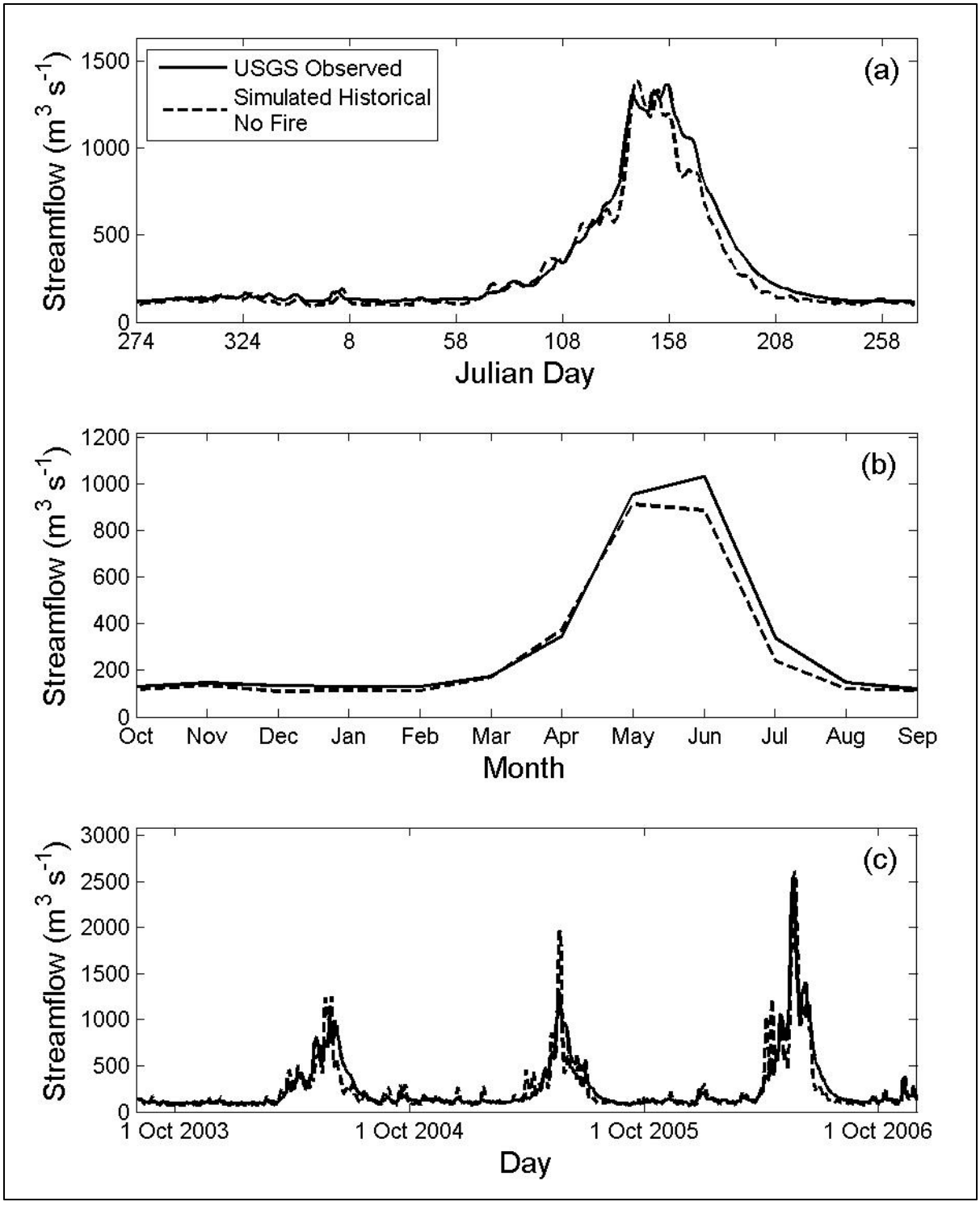


Figure 6. Observed and simulated discharge for the evaluation period at the outlet of Basin One for (a) the average Julian day, (b) average month, and (c) three years of daily flows.

Although there are few sediment yield observations in the SRB, the short- and long-term sediment rates from Kirchner et al. (2001) provided an evaluation of the general magnitude of VIC-WEPP model sediment rates. Figure 7 shows the VIC-WEPP model average annual sediment yield for the historical no fire condition over the entire SRB. Individual grid cell values ranged from 0 t $ha^{-1}$ to 774 t $ha^{-1}$ with a basin average of 10 t $ha^{-1}$. Figure 8 shows the VIC-WEPP model and Kirchner et al. (2001) sample short- and long-term yields from the seven sample locations. The average VIC-WEPP model yield corresponding with the seven locations was 4.37 t $ha^{-1}$, the average short-term yield was 0.12 t $ha^{-1}$, and the average long-term yield was 2.14 t $ha^{-1}$. Based on this evaluation, the VIC-WEPP model predicts yield within one order of magnitude for short-term yields and the same order of magnitude for long-term yields.

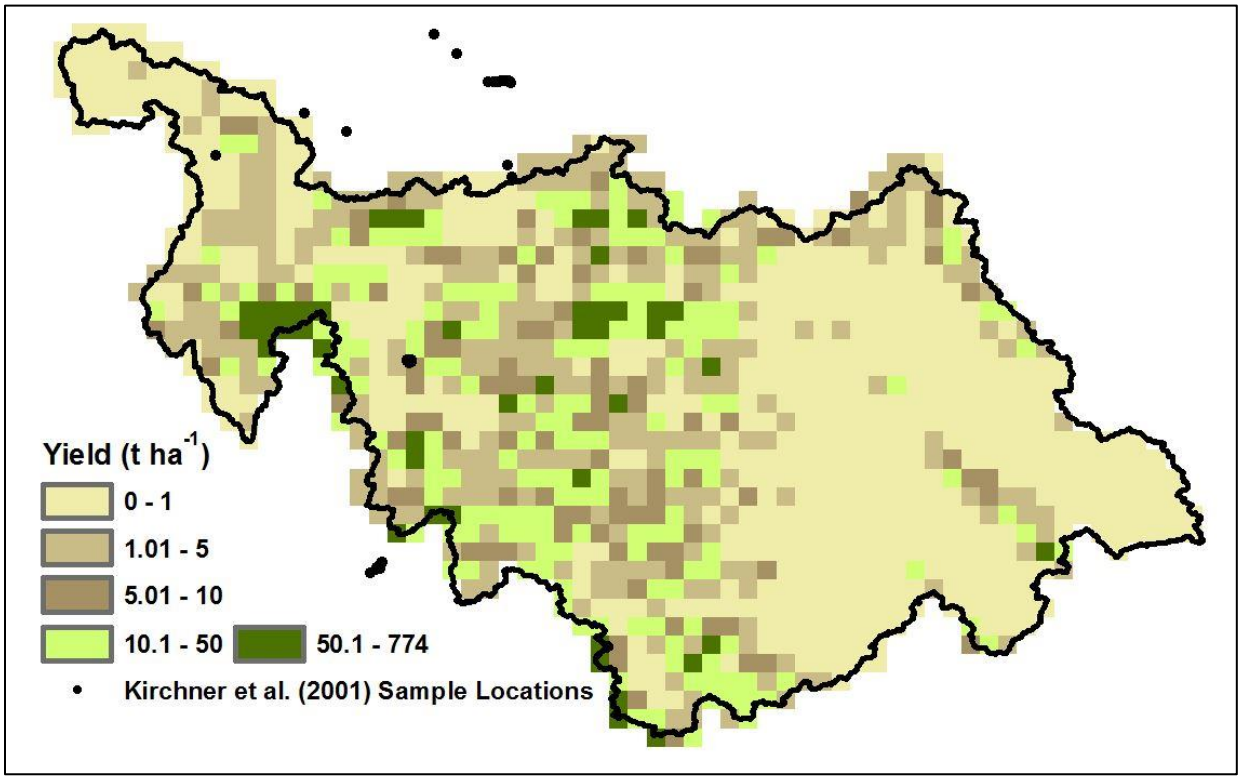


Figure 7. Average annual sediment yields predicted by the VIC-WEPP model for the entire SRB for the historical no fire condition. Black points represent Kirchner et al. (2001) sample locations.

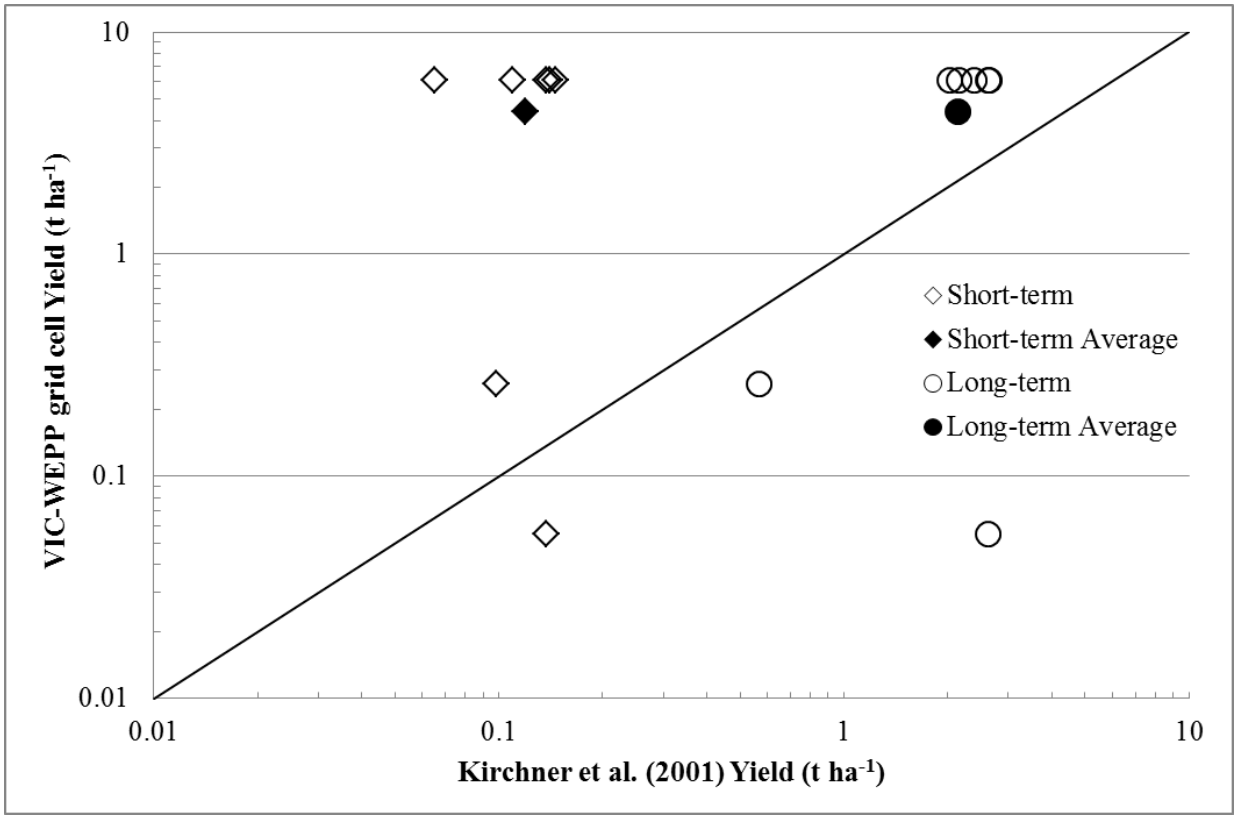


Figure 8. Average annual sediment yield comparison between the VIC-WEPP model and Kirchner et al. (2001) short and long term time scales.

## 4.2 Model Inter-comparison

### 4.2.1 Hillslope Comparison

Combining all no and high fire severity conditions for the model comparison, hillslope yield averages were used to produce tabulated data and gradient plots which compared both models and fire conditions. The VIC-WEPP model predicted average annual hillslope sediment yield as 0.85 t $ha^{-1}$, which was more than double the yield of Disturbed WEPP, which estimated average sediment yield as 0.36 t $ha^{-1}$. Figure 9 provides a cumulative distribution function (CDF) plot of all hillslopes and shows a concentration of sediment yield for Disturbed WEPP between 0.01 and 10 t $ha^{-1}$ whereas shows the VIC-WEPP model range from nearly zero to 125 t $ha^{-1}$.

Although the CDF curves in Figure 9 show that the VIC-WEPP model was generally underestimating erosion compared to Disturbed WEPP, the large yields from the VIC-WEPP model outweigh the smaller yields. The difference in each model's range represents the relative sensitivity of each model which is discussed in Section 4.2.2.

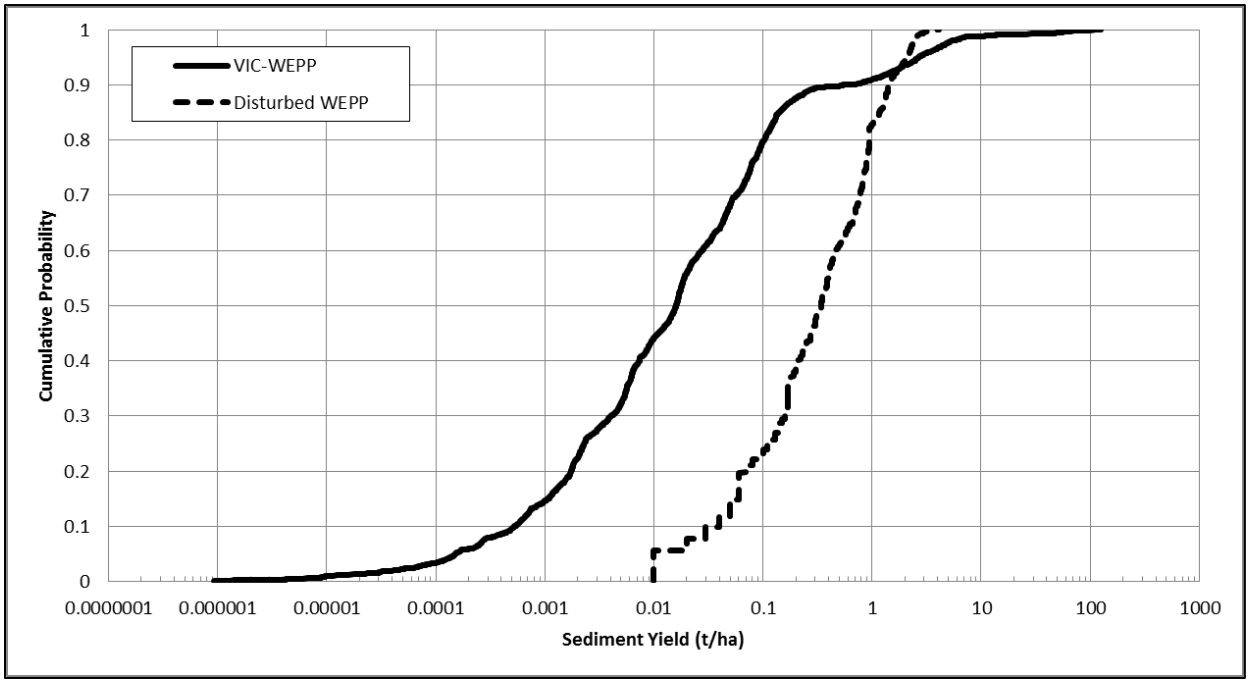


Figure 9. CDFs of annual average sediment yields for all hillslopes for both the VIC-WEPP model and Disturbed WEPP.

Figure 10 shows a comparison between the average annual sediment yields of the two models where symbols are used to identify no or high fire severity. Likewise, Figure 11, Figure 12, and Figure 13 compare the two models' yields for average annual precipitation, average slope, and vegetation type. Disturbed WEPP reported sediment yields with a precision of 0.01 t $ha^{-1}$ so smaller values were not represented. The fire severity, average annual precipitation, and average slope plots showed a gradient of yields on both sides of the one-to-one line which implied that these variables were not likely to be the cause for any major differences between the

models. However, Figure 13 shows stronger partitioning of results between each of the four vegetation types, suggesting that differences in how vegetation was treated between the models were an important source of model differences.

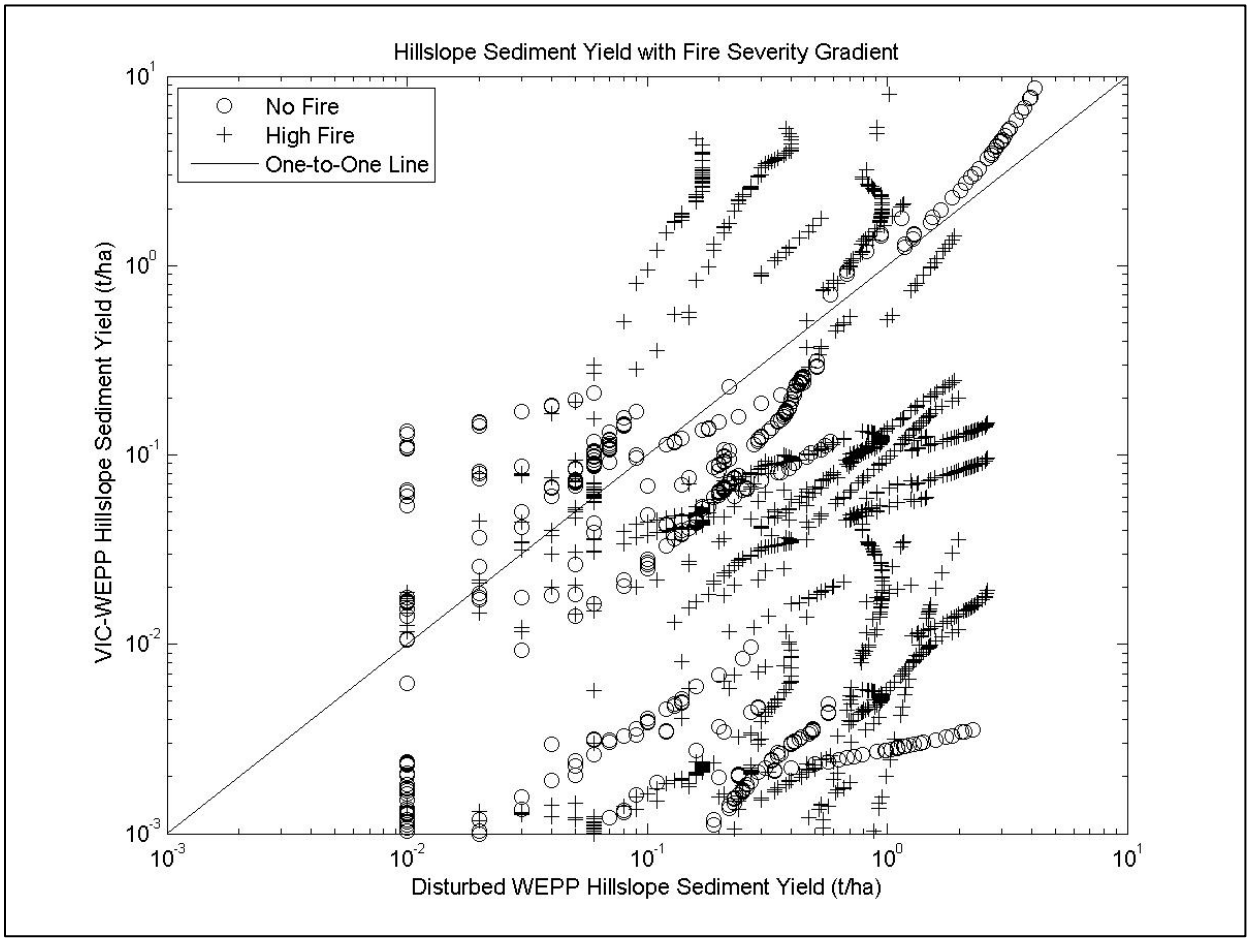


Figure 10. Scatter plot of annual average sediment yield for the VIC-WEPP model (vertical axis) and Disturbed WEPP (horizontal axis) where the symbols represent gradients for fire severity.

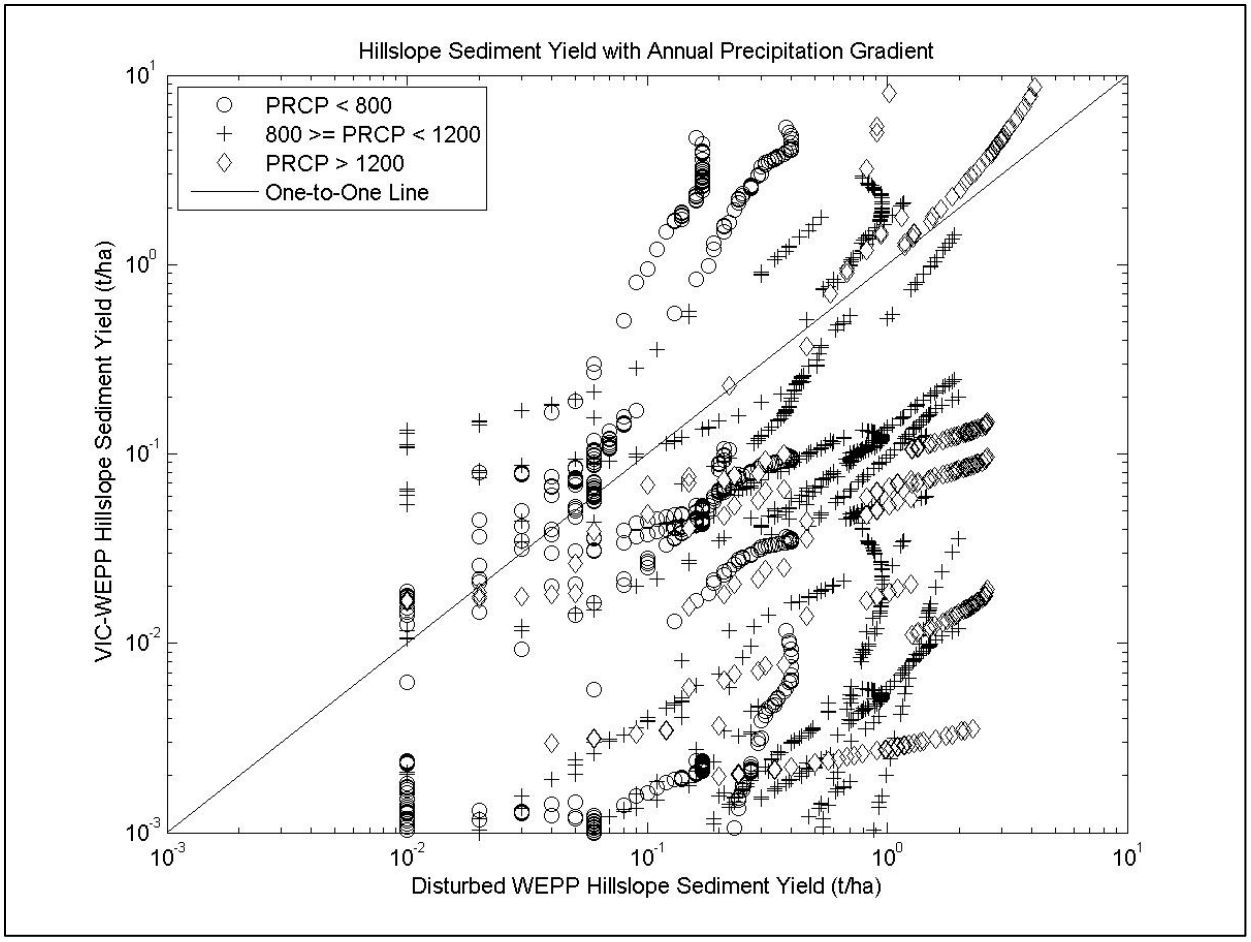


Figure 11. Scatter plot of annual average sediment yield for the VIC-WEPP model (vertical axis) and Disturbed WEPP (horizontal axis) where the symbols represent gradients for average annual precipitation.

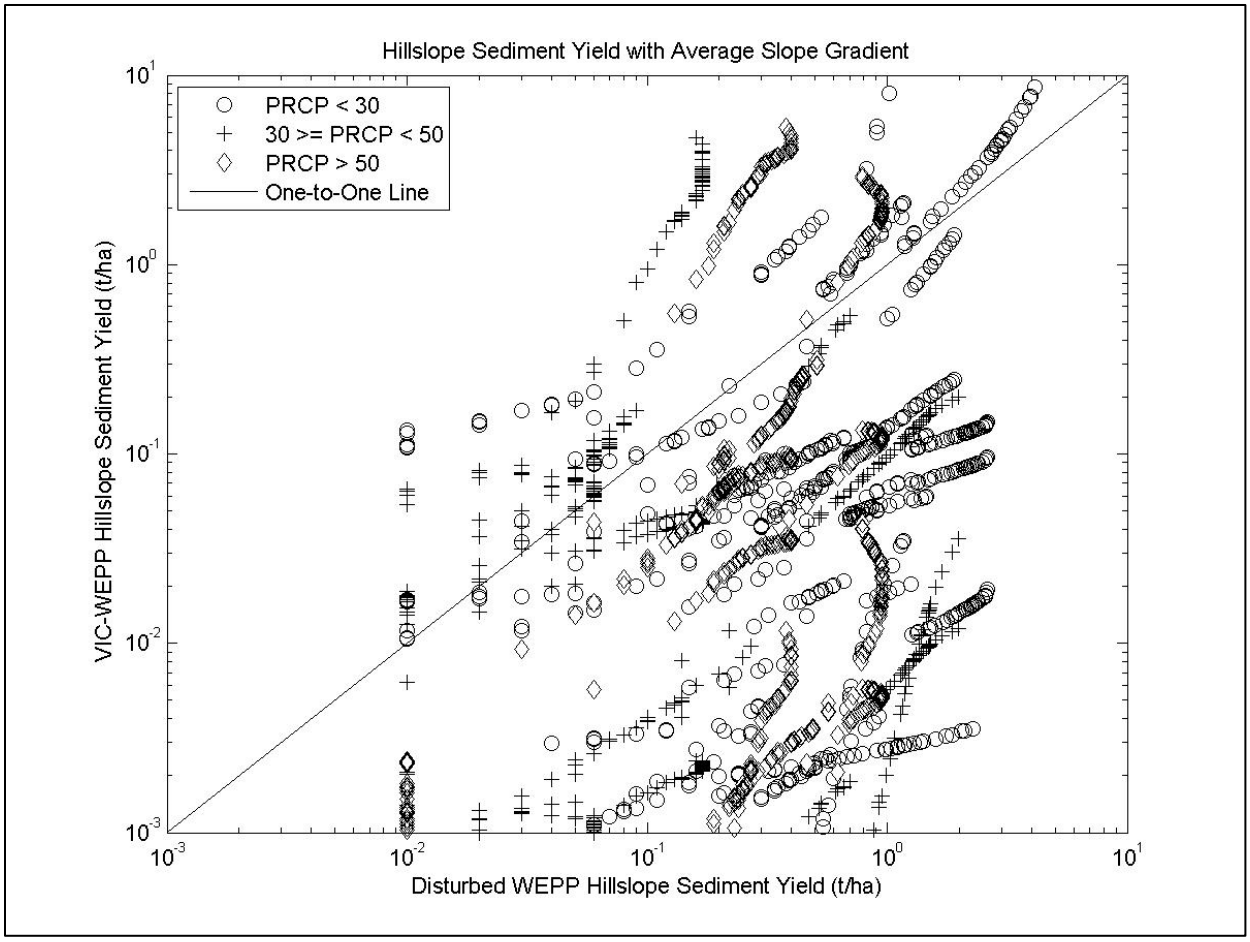


Figure 12. Scatter plot of annual average sediment yield for the VIC-WEPP model (vertical axis) and Disturbed WEPP (horizontal axis) where the symbols represent gradients for average slope.

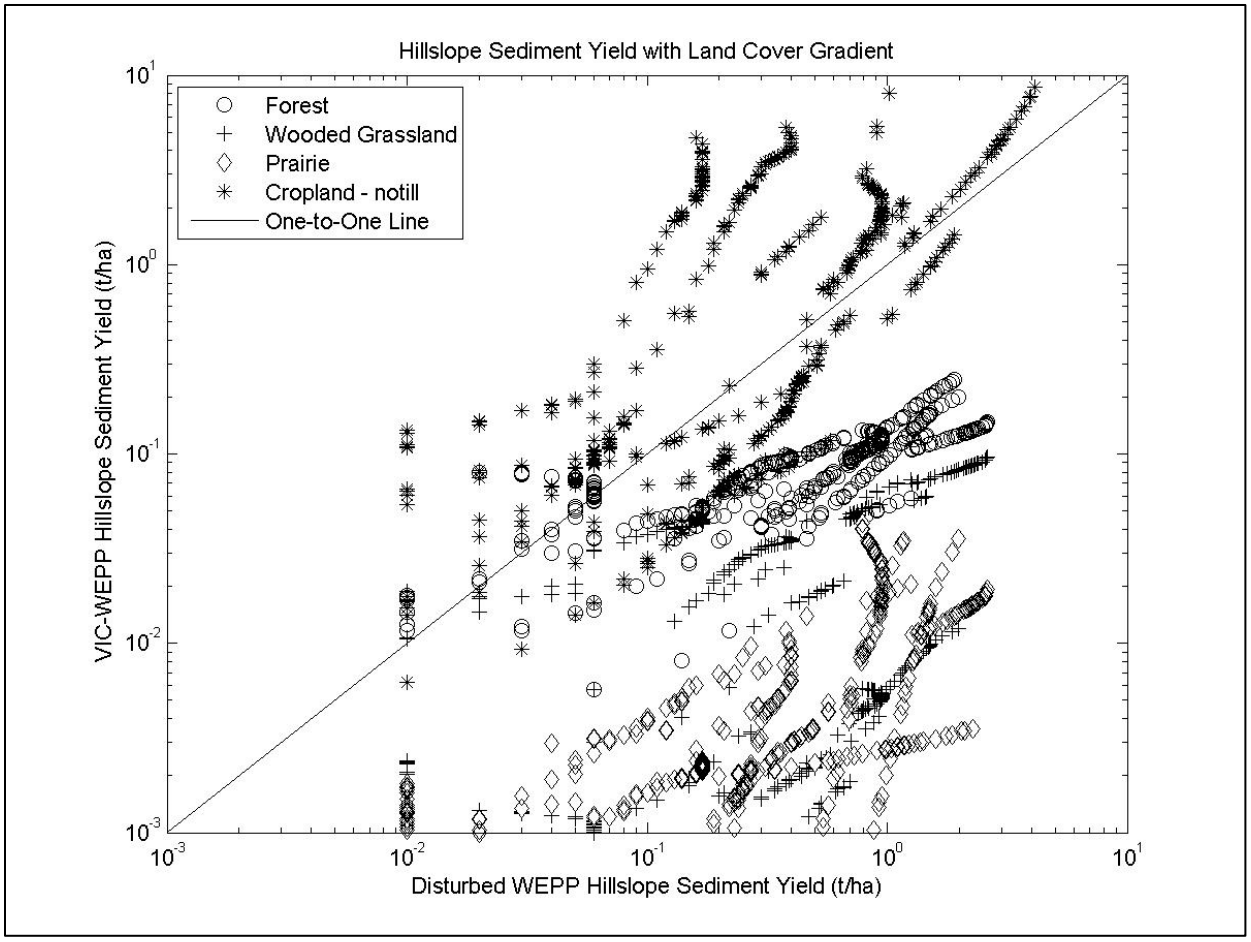


Figure 13. Scatter plot of annual average sediment yield for the VIC-WEPP model (vertical axis) and Disturbed WEPP (horizontal axis) where the symbols represent gradients for the VIC-WEPP model land cover vegetation type.

### 4.2.2 Hillslope Sensitivity

The sensitivity tests for both models showed which parameters were more influential on erosion for each model (Table 13). For Disturbed WEPP, the sensitivity of cover indicated that yield decreased with increased cover percent. This makes sense intuitively because larger amounts of vegetation on the soil surface causes increased tc due to the presence of root systems and biomass. The largest changes in yield were nearly -0.5 t $ha^{-1}$ for ground cover inputs. Opposite to cover, an increased slope increased the erosion which also was intuitive because a

steeper slope increases the potential for detachment of particles. The largest yield difference that slope contributed was 5 t $ha^{-1}$. Similar with slope, yield increased with increased slope length by 7.1 t $ha^{-1}$. Similar to cover, increased hydraulic conductivity decreased yield. An increased conductivity results in a larger percent of water infiltrating into the soil column leaving less water to act as runoff which was the main driver of sediment yield. The largest difference in yield impacted by hydraulic conductivity was -0.64 t $ha^{-1}$.

The two values used for rill erodibility, 0.0003 s $m^{-1}$ and 0.0004 s $m^{-1}$, were from the loam soil texture with Poor grass and Low severity fire treatments, respectively. The largest difference on erosion between the two rill erodibility values was 0.07 t $ha^{-1}$. Critical shear only had one combination of soil texture and treatment type in Disturbed WEPP inputs options that allowed for tc values to be different with all other factors remaining constant. The silt loam and Thin or young forest input was compared to the loam and Low severity fire input (both using 10% cover and 100% slope) which resulted in a yield change of -0.41 t $ha^{-1}$ for a 0.5 N $m^{-2}$ increase in tc (Table 13). Although other factors were present in different locations, such as elevation and temperature (which impact runoff via snowmelt), annual precipitation was the main variable considered in driving the differences in yield for the sensitivity of location on erosion. The yield calculated in Table 13 was from inputs of silt loam soil texture, Short grass treatment, 10% cover, and 100% slope which showed an increased yield of 9.56 t $ha^{-1}$.

For the VIC-WEPP model sensitivity, the Ki increased yield by 5.08 t $ha^{-1}$. Kr showed no impact on yield because all values tested remained at the control simulation result. It was expected that yield increased with increased Ki and Kr values because the soil would be more erodible with higher values. Kr did not affect yield within the range of values used for this sensitivity but may contribute to changes at higher values. Yield was changed by -0.013 t $ha^{-1}$ for

increased tc. This made sense based on physical processes because an increased tc (more energy required to erode soil) should result in less erosion which this sensitivity captured. As Kc increased, the yield decreased which was similar to the Disturbed WEPP sensitivity. Over the range of Kc values, the VIC-WEPP model showed a change of -0.125 t $ha^{-1}$ in yield (Table 13).

Twelve slopes, including the control value, were selected to test for sensitivity in the VIC-WEPP model. An increase of 21 t $ha^{-1}$ in yield was shown over the range of slope values selected. The sensitivity of yield to slope length was opposite compared to Disturbed WEPP results. For the VIC-WEPP model, slope length had a change in yield of -12.6 t $ha^{-1}$ over the same range of slope lengths from Disturbed WEPP. Further investigation showed the both models produced increased amount of sediment mass with increases in slope length. The likely explanation for the differences between the two models is the difference of hillslope width which correlates to different hillslope areas. For both models, the hillslope area and sediment mass increased with increased slope length although for the VIC-WEPP model the rate at which area increased had larger impact on yield than the rate at which mass increased (resulting in a decrease in yield) and opposite for Disturbed WEPP which showed the mass rate impacting yield more than the area rate (resulting in an increase in yield). These differences could be contributed to the differences in erosion model versions used in each model (see Section 3.3.1). Similar to cover, LAI effected yield by increasing the vegetation present in the system which increased the canopy which reduces the force of impact from raindrops and eventually decreased the yield. There was a -2.1 t $ha^{-1}$ change in yield when LAI was increased from 40% to 160% of the control value. The most sensitive parameter tested in the VIC-WEPP model was the land cover input. The first three types (forest, wooded grassland, and prairie) produced the same yield (5.1 t $ha^{-1}$) whereas cropland and bare soil produced 494 t $ha^{-1}$ and 2,056 t $ha^{-1}$, respectively, resulting in a

yield change of 2,051 t $ha^{-1}$. Last, the changes in yield based on changes in location (average annual precipitation) was 10.2 t $ha^{-1}$ from the lowest average annual precipitation to the highest for the VIC-WEPP model sensitivity on climate (Table 13).

Table 13 provides a summary of the yield changes for each of the parameters considered in both sensitivity tests. For Disturbed WEPP, the differences in average annual precipitation have the largest effects on yield followed by slope length and slope. For the VIC-WEPP model, the land cover type was most influential on erosion followed by slope length, slope, and climate. Comparing the five parameters that were similar between the two models (average annual precipitation, slope, hydraulic conductivity, tc, and Kr), the rate of yield change was calculated as the quotient of yield change and range of parameter. Comparing the rate of change between similar parameters described the relative sensitivity of each model to that specific parameter. Disturbed WEPP was more sensitive than the VIC-WEPP model to hydraulic conductivity, tc, and Kr. The VIC-WEPP model was more sensitive to changes in land cover, average annual precipitation, slope length, and slope. The change in yield for the VIC-WEPP model land cover was two orders of magnitude greater than all other parameters which implied yield from VIC-WEPP model applications would be greatly impacted by land cover type.

Table 13. Summary of sensitivity of sediment yield to changes in model parameters for both models.

| Input Parameter | Disturbed WEPP | | | VIC-WEPP | | |
|---|---|---|---|---|---|---|
| | Range of Values | Yield Change ($t\ ha^{-1}$) | Rate of Yield Change (fraction) | Range of Values | Yield Change ($t\ ha^{-1}$) | Rate of Yield Change (fraction) |
| Average Annual Precipitation (mm) | 598-1296 | 9.56 | 0.0137 | 598-1296 | 10.2 | 0.0146 |
| Slope (%) | 1-100 | 5.00 | 0.051 | 0.1-110 | 21.0 | 0.191 |
| Slope length (m) | 5-95 | 7.10 | 0.079 | 5-95 | -12.6 | -0.140 |
| Hydraulic Conductivity ($mm\ day^{-1}$) | 144-672 | -0.64 | -0.0012 | 300-2700 | -0.125 | -0.0001 |
| Cover (%) | 0-100 | -0.50 | -[a] | - | - | - |
| Critical Shear ($N\ m^{-2}$) | 0.5-1.0 | -0.41 | -0.82 | 0.45-1.05 | -0.013 | -0.02 |
| Rill Erodibility ($s\ m^{-1}$) | 0.0003-0.0004 | 0.07 | 700 | 0.0001-0.0007 | 0.00 | 0.00 |
| Land Cover | - | - | - | Forest, wooded grassland, prairie, cropland, and bare soil | 2051 | - |
| LAI (fraction) | - | - | - | 0.4-1.6 | -2.1 | - |
| Interrill Erodibility ($kg\ s\ m^{-4}$) | - | - | - | 300000-1500000 | 5.08 | - |

[a] – indicates these data were not calculated because the parameter was not tested in both models.

## 4.3 Climate Change and Fire Impacts on Streamflow

The potential impacts of climate change on the streamflow hydrographs were explored by simulating the VIC model for multiple climate scenarios (see Section 3.5) from 2041-2070. The future

streamflow was compared to simulations of streamflow over the historical period (1981-2010) with the no fire severity condition. The future climate scenarios were averaged for each fire severity condition (see Figure 14).

Basin One average future scenario streamflows with all four fire severity conditions is shown in Figure 14 for average Julian day and average monthly streamflows. Under no fire conditions for Basin One (see Figure 1 for location), climate change impacted streamflow by decreasing the peak flow and shifting it earlier in the season compared to the historical no fire condition streamflow (Figure 14). For each of the future streamflow fire conditions, the magnitude of peak streamflow increased with each increase in fire severity with the high fire condition peak magnitude greater than the historical peak magnitude. The future low and moderate fire conditions did not change the timing of peak streamflow compared to the future no fire condition on the daily time-step (Figure 14(a)) but on a monthly average increased the amount of streamflow earlier in the season (Figure 14(b)). The future high fire condition had a shift in peak streamflow compared to the historical no fire condition by over 50 days earlier in the season (Figure 14). Sridhar et al. (2012) showed Basin One peak flow timing shift to earlier in the season by 10 days with future climate change whereas this study showed a similar shift in peak flow timing by nearly 25 days with the average future no fire condition. The increase in peak flow magnitude due to increases in fire severity was due to less vegetation available to store water and the surface being more repellent due to wildfire which caused an increase in runoff. The decreased vegetation and increased surface repellency was caused by the changes in the post-fire adjustment factors LAI and Kc for each fire severity condition (see Section 3.1.3.7). The hydrographs for the other three basins are shown in the Appendix.

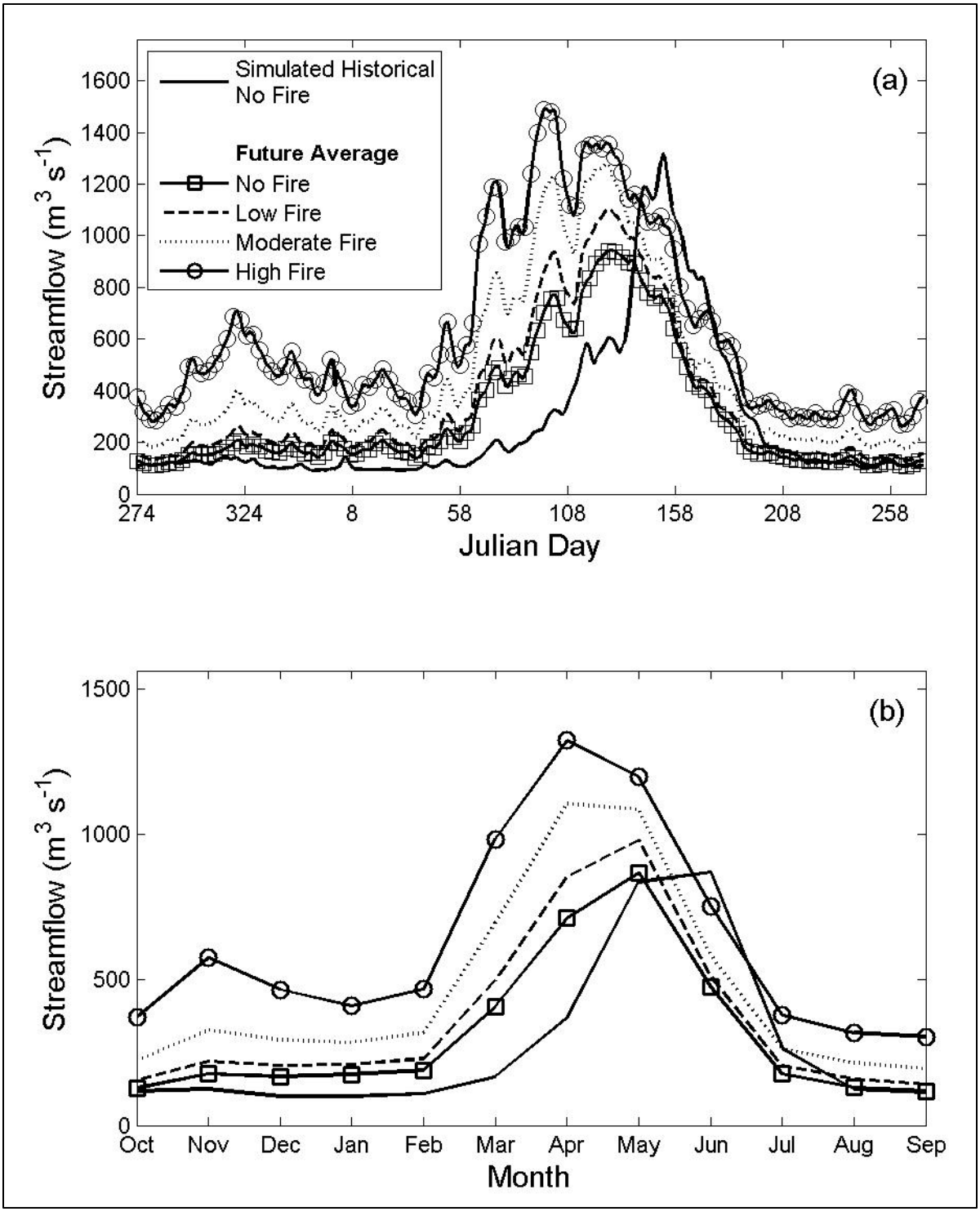


Figure 14. Future streamflow compared to historical simulated streamflow for no, low, moderate, and high fire severity conditions for Basin One for (a) the average Julian day streamflow (beginning on October 1) and (b) the average monthly streamflow. The future streamflow is the average of the five future scenarios (see Section 3.5).

## 4.4 Climate Change and Fire Impacts on Erosion

To be able to simulate more scenarios while minimizing computational requirements, erosion simulations were conducted on two areas. The first area covered the entire SRB and included one future scenario (MIROC5 RCP4.5). The second area consisted of 80 grid cells within a representative range of the entire basin for annual precipitation, slope, land cover, and sediment yield change based on results from the first area. The MIROC5 RCP4.5 scenario was selected to show the mid-range future climate projection. Average annual sediment yield impacts across the SRB due to changes in both climate and fire conditions were examined and are summarized in Figure 15. Table 14 describes how each of the maps in Figure 15 was calculated. Maps (c) and (d) from Figure 15, showing the climate effect on erosion, have yield changes that are much less then maps (a) and (b), which show the effect of fire on erosion. Also, the most extreme changes for all maps are -227 t $ha^{-1}$ and 927 t $ha^{-1}$. Although the rates are two orders of magnitude greater than the long-term yields from Kirchner et al. (2001) (see Section 4.1), these rates represent the effects of extreme wildfire conditions which resulted in expected extremely high yield rates compared to observed and long-term yields.

Table 14. Summary of calculations used for producing the yield change erosion maps for Figure 15. To clarify, one of the two axes of variability is historical climate or future climate while the other axis is no fire or high fire.

| Panel | Erosion Calculation for Figure 15 |
|---|---|
| a | (historical high fire) – (historical no fire) |
| b | (future high fire) – (future no fire) |
| c | (future no fire) – (historical no fire) |
| d | (future high fire) – (historical high fire) |

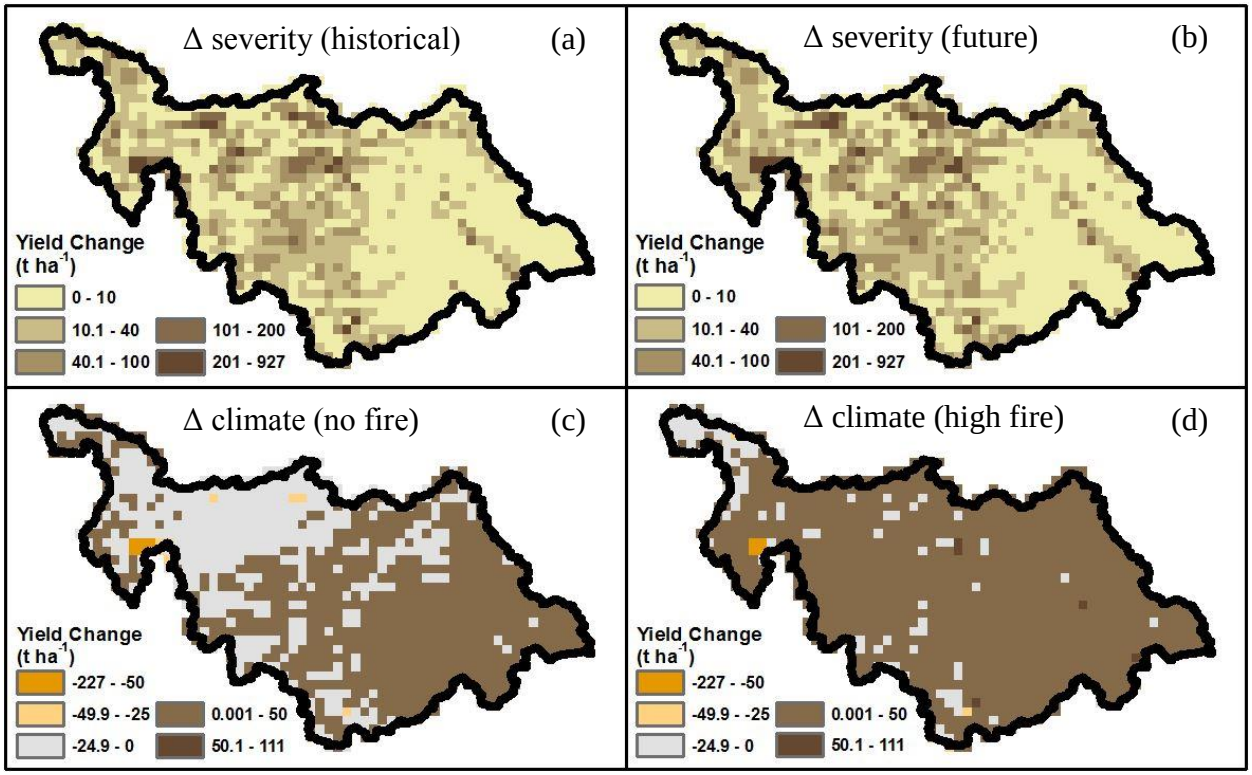


Figure 15. Average annual sediment yield changes due to changes in fire conditions for (a) historical and (b) future climates; and changes due to climate for (c) no fire and (d) high fire severities.

There were widespread differences in yield across the SRB. The most important factors contributing to the heterogeneity of erosion were those identified as important factors from the sensitivity test (land cover, slope length, slope, and precipitation). As land cover increased yield from 5 t $ha^{-1}$ to 490 t $ha^{-1}$ from forest to cropland conditions (at 20% slope) and average annual precipitation (from 1,048 mm to 1,296 mm) impacted yield from 5 t $ha^{-1}$ to 11 t $ha^{-1}$, the potential for erosion to be very large with the extreme conditions of cropland, high slope, and high precipitation were evident. Also, the large yield changes may have been caused from the method used to incorporate fire conditions into the VIC-WEPP model. By adjusting the erodibility factors, Kc, and LAI, the conditions in the model superimposed ideal post-fire forest conditions on every hillslope and land cover type for all time periods even though such conditions are not likely to be widespread throughout the basin

spatially and temporally and different land cover types have different post-fire adjustments (Robichaud et al. 2007).

To help understand the source of the large magnitudes of erosion, an analysis was performed on the distribution of sediment yield to each land cover type by area for the model grid cells with greater than 100 t $ha^{-1}$ for the historical high fire severity condition. From the total 1,153 model grid cells in the SRB, 101 gave average annual sediment yield over 100 t $ha^{-1}$ with the largest being 1,609 t $ha^{-1}$. From these 101 model grid cells, the average area for each land cover type in each model grid cell was calculated. Along with the average area, the average sediment contribution from each of the land cover types for each model grid cell was calculated. Table 15 provides the average percent of total sediment yield for one percent of total area for the analysis of the 101 model grid cells. For the average model grid cell, 0.053 t $ha^{-1}$ was generated for every 1% of the area that was forest, 0.049 t $ha^{-1}$ was generated for every 1% of the area that was wooded grassland, 0.013 t $ha^{-1}$ was generated for every 1% of the area that was prairie, 7.0 t $ha^{-1}$ was generated for every 1% of the area that was cropland, and 27 t $ha^{-1}$ was generated for every 1% of the area that was bare soil. This implies that even with small fractions of a study domain as cropland (such as the SRB), this VIC-WEPP model framework provides large magnitudes of sediment yields that are mainly driven by cropland land cover. An important factor to mention is the VIC-WEPP model erosion results were not routed downstream into rivers which could decrease the yields in this study greatly because not all sediment may be transported to rivers.

Table 15. The percent of total sediment for one percent of total area over the 101 model grid cells with yield greater than 100 t $ha^{-1}$ for the historical high fire severity condition.

| Land Cover | Percent of Total Sediment Yield for every One Percent of Total Area (%) |
|---|---|
| Forest | 0.053 |
| Wooded Grassland | 0.049 |
| Prairie | 0.013 |
| Cropland | 7.0 |
| Bare Soil | 27 |

Additional future scenario simulations were done over a test area in the central SRB (see Figure 1). Figure 16 shows the yield results from six climates and four different fire severities over this test area. The top row shows all four severities for the historical climate and similar for the remaining rows for the future climate scenarios. The future scenarios in Figure 16 are ordered from most extreme in precipitation difference to least extreme (see Figure 2). There is a general trend from left to right on Figure 16 showing that with increases in fire severity the yield increases. The spatial distribution of which grid cells increase the most was similar regardless of climate scenario but the magnitude of yield change varied for each climate scenario due to the differences in climate variability. As discussed above with Table 15, the differences in yield magnitudes are associated with the percentage of hillslopes that are cropland and bare soil within the model grid cell.

The change in yield from one scenario to another was important to understand the relative sensitivity of wildfire and climate change on yield. Figure 17 shows the yield change from the no fire condition to a low, moderate, or high condition while keeping the climate constant. The maps in Figure 17 are very similar to the corresponding maps in Figure 16 not only with spatial distribution but also with magnitude. Keeping the fire condition constant, Figure 18 shows the yield changes from the historical climate to the different future scenarios. Different from before, the yield had negative values

which represented areas in which the future climate produced erosion rates less than the simulated historical rates. The yield changes in Figure 18 are roughly one order of magnitude less than the changes between fire severities as in Figure 17.

Along with the factors affecting the differences in yield magnitudes, understanding the factors affecting when erosion occurs can provide insight into how erosion could change in the future. Sediment yield on a daily time-step was compared to rainfall, snowpack cover, and snowmelt to show the distribution of when erosion was occurring. Table 16 shows the average sediment yield for days when yield occurred during rainfall on snowpack with snowmelt conditions and rainfall with no snowpack conditions. The values in Table 16 are averaged for all days in the 30-year time period for all climates over the test area (see Figure 1). First, for the historical case, there was an average yield of 0.690 t $ha^{-1}$ for days that generated yield when there was rainfall on snowpack with snowmelt compared to only 0.084 t $ha^{-1}$ for days that generated yield when there was rainfall and no snowpack. This showed that more of the historical yield occurred when there was snowpack present compared to when there was no snowpack. The average percent of days with snowpack present during days generating yield was 56.0% (Table 16). Second, considering the future climate scenarios, the average yield when there was rainfall on snowpack with snowmelt was less than the historical case for each future scenario. The average yield when there was rainfall with no snowpack was greater than the historical case for each future scenario which showed that there was a shift in when erosion was occurring in future climates although rainfall on snowpack with snowmelt conditions continued to show greater average yield than rainfall with no snowpack. This was also captured in the average percent of days with snowpack present as shown in Table 16 with less snowpack present for each of the future scenarios compared to the historical case. This analysis showed that rainfall on snowpack

conditions played a significant role in runoff production and thus the timing of sediment yield generation.

Table 16. Average sediment yield for days when yield occurred during rainfall on snowpack with snowmelt conditions and rainfall with no snowpack conditions. Also, the average percent of days with snowpack present during days generating yield is shown.

| Climate with No Fire Severity Condition | Average Sediment Yield for Days Generating Yield with Specific Hydrologic Conditions in Test Area (t $ha^{-1}$) | | Average Percentage of Days with Snowpack Present during Days Generating Yield (%) |
|---|---|---|---|
| | Hydrologic Condition | | |
| | Rainfall on Snowpack with Snowmelt | Rainfall with no Snowpack | |
| Historical | 0.690 | 0.084 | 56.0% |
| CanESM2 RCP8.5 | 0.557 | 0.134 | 38.8% |
| GFDL-ESM2G RCP8.5 | 0.605 | 0.174 | 44.3% |
| MIROC5 RCP4.5 | 0.631 | 0.122 | 42.6% |
| BCC_CSM1.1 RCP8.5 | 0.489 | 0.123 | 49.0% |
| INMCM4.0 RCP4.5 | 0.627 | 0.119 | 53.1% |

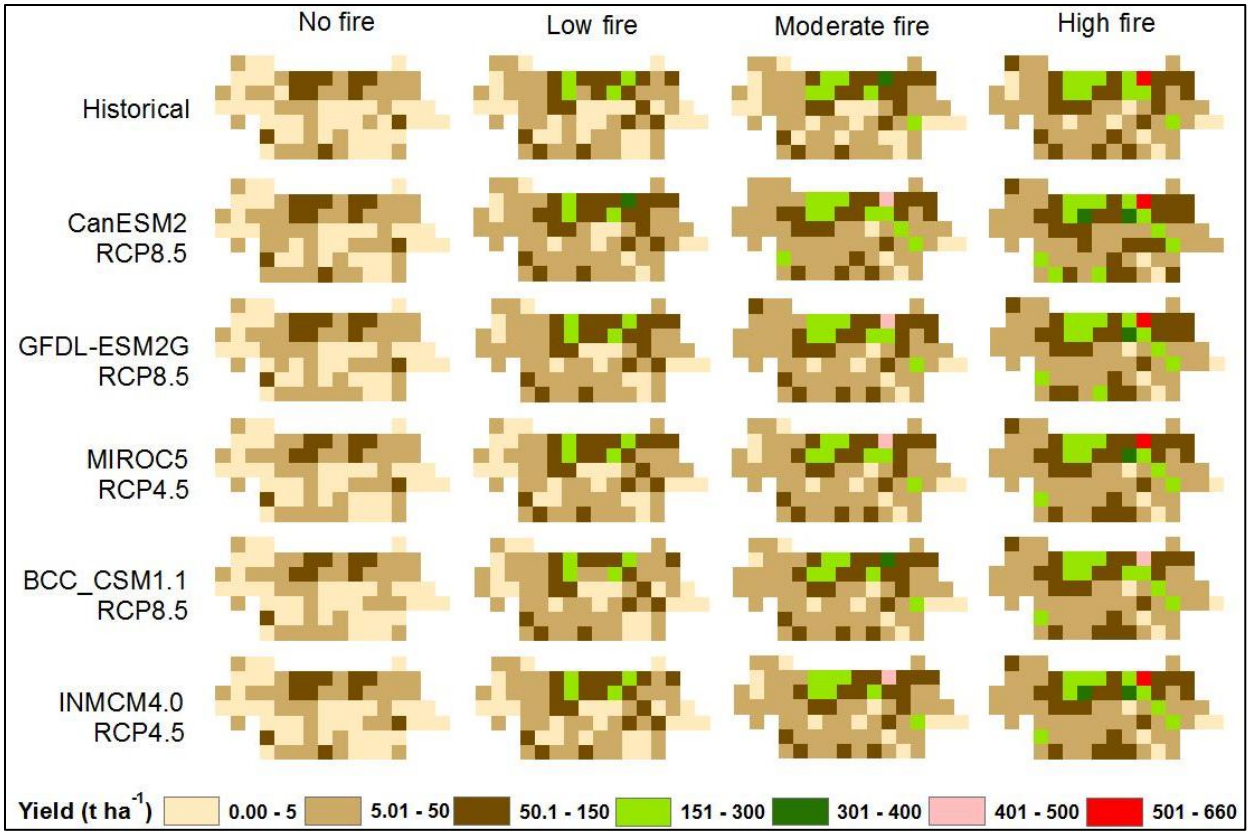


Figure 16. Erosion yield from six climates (rows) and four different fire severities (columns) for test area (see Figure 1 for location).

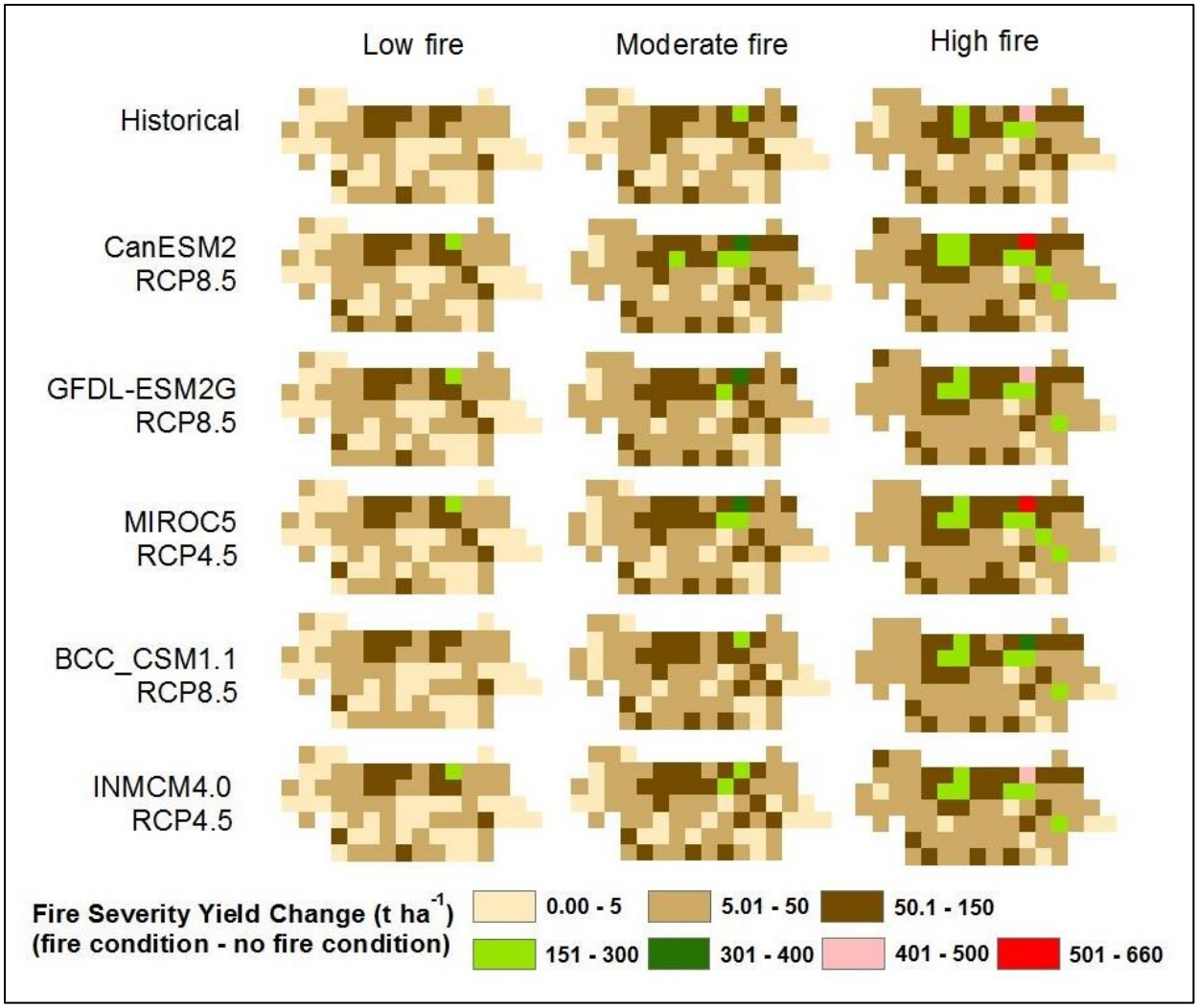


Figure 17. Erosion yield change from the no fire condition to a low, moderate, or high condition while keeping the climate constant.

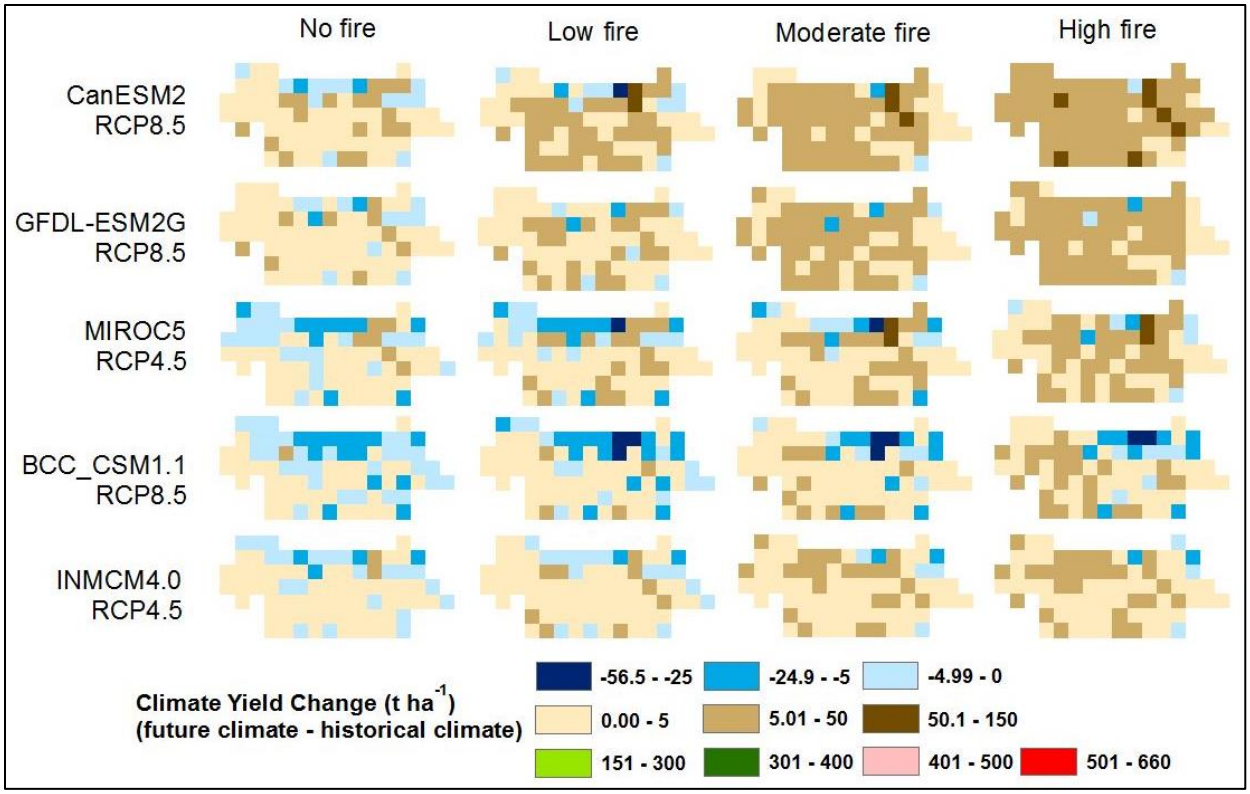


Figure 18. Erosion yield change from the historical to future climate while keeping the fire condition constant.

The test area erosion maps provide insights on the interactions of climate, fire severity, and post-fire erosion. Although the extreme wildfire conditions overwhelmed the climate contributions to erosion, the climate scenarios were producing negative and positive yield changes which suggested climate has a significant impact on erosion variability. On the daily time-step, large magnitudes of sediment yields were mainly driven by cropland land cover and the most sediment yields occurred during rainfall on snowpack conditions. Also, these maps show the possibility of modeling physically-based erosion at large scales which has important impacts on future climate change and post-fire erosion studies.

# CHAPTER FIVE

# LIMITATIONS AND FUTURE WORK

With all modeling studies there are limitations and uncertainties involved. One of the largest limitations to this study was the lack of fine resolution observed erosion data and streamflow sediment concentrations. There were some observed datasets available, for example Disturbed WEPP had been calibrated and evaluated at 24 test plots in western Montana for post-fire erosion by Spigel and Robichaud (2007), the study by Kirchner et al. (2001) discussed in Section 3.2, and the USGS had limited streamflow concentrations of suspended sediment. Efforts to increase the observed data available would increase the ability to calibrate and evaluate the erosion processes in the VIC-WEPP model. If streamflow sediment concentrations were used in calibration, the VIC-WEPP model would need an erosion routing scheme added to the modeling framework.

Another caveat in the VIC-WEPP model that was important for this study was that land cover types for individual representative hillslopes were determined by a coarse scale resolution dataset. Unlike slope, which was rescaled to better represent the actual fine scale slopes, land cover type was not adjusted to better represent the actual distribution of land cover within a grid cell. The sampling method used in this study could have produced a representative hillslope with cropland land type with slopes over 100%. Although the sampling process determines VIC-WEPP model grid cell sediment yield proportionally based on the land cover type distribution (for example, if a model grid cell is 90% forest and 10% cropland, the model grid cell yield will be 90% from the forest hillslopes and 10% from the cropland hillslopes), because the cropland land cover has much larger yields (see Section 4.2.2) than forest land cover, the proportionally sampling is potentially

overestimating the model grid cell sediment yield. Another important limitation related to cropland land cover overwhelming the majority of forest erosion is how post-fire adjustment factors from forest conditions are applied to cropland land cover imposing unrealistic post-fire conditions in cropland areas which causes increased yield.

Another limitation to this study was that it did not incorporate the transient effects of fires on streamflow or erosion. This study applied historical fire severity conditions to the entire SRB for all time-steps without addressing changes in future fire behavior (frequency or severity) or regrowth after a fire. Future work that would provide an improvement to the modeling framework could include a fire model that has the ability to model fire ignition for specific areas and communicate the fire's location, duration, severity, and regrowth while the VIC-WEPP model adjusts the Kc, LAI, and erodibility factors according to the current fire conditions. This would demonstrate the effects of individual fires as well as all fires aggregated over a season (with regrowth) on erosion at large-scales using a physically-based fire model rather than the entire basin overlay approach used in this study.

Another step in developing the modeling framework would be to use fine scale (30 m) slope and land cover dataset to determine the representative hillslopes used in the erosion process. This would reduce the sampling uncertainty but methods would need to be developed to manage the large increase in spatial data (nearly 50,000 hillslopes to sample from for each grid cell compared to the 225 used in this study). Related to hillslope sampling is the large computational time required to simulate the erosion process over large-scales. A study on the impacts of the number of hillslopes sampled on yield could provide insight in how to reduce simulation run-time. Although this method would not be feasible for the entire PNW, it could allow development on how to better sample coarse slope and land cover data.

Also, additional work to determine the contribution of rill and interrill erodibility to the total erosion would increase the understanding of which mechanism (rainfall or channelized flow) effects yield more at various times in the year.

For the journal article that will be submitted based on this thesis, additional work will include exploring methods to better include this erosion process in regional-scale earth system modeling frameworks. This will incorporate the suggested future work related to the impacts of the number of hillslopes sampled on yield compared to the simulation run-time required.

# CHAPTER SIX

# CONCLUSIONS

The VIC-WEPP model was applied over the SRB to consider the relative sensitivity of extreme wildfire events and climate change on erosion at large-scales. The VIC model was calibrated and evaluated for streamflow against USGS observed streamflow records showing E values greater than 0.60 for most basins in both time periods. Streamflow results showed an earlier shift in peak flow by one to two months for future climate scenarios. Timing of peak flow shifted to earlier in the season for all average future streamflow fire severity conditions. Also, the magnitude of peak flow increased from no to high fire severity at each severity.

A model comparison of the VIC-WEPP model was performed with Disturbed WEPP to check for similar orders of magnitude in erosion rates. Also, sensitivity tests showed the impact of key parameters on erosion for each model. The VIC-WEPP model key factors effecting erosion in the SRB were land cover type, slope length, slope, and average annual precipitation. To incorporate the effects of wildfire, model development provided a method to perturb a specific fire severity on the entire simulation. For future scenarios, this study only considered meteorological impacts on post-fire erosion and did not incorporate changes in future fire occurrence or burn severity.

Sediment yield results showed fire severity conditions impacted the magnitude of yield by one to two orders more than climate change. However, climate change effects on yield were more diverse because decreases and increases in change of yield occurred due to changes in precipitation. Yield followed a clear trend when only fire severity impacts were represented. For every scenario, the yield change increased from low to high fire conditions. Considering the climate impacts

on yield, the change was more diverse and dependent on precipitation changes. Although, even with climate changes causing decreased yield, increased fire severity overtook the climate change effects. Erosion was more sensitive to extreme wildfire events but climate change had more diverse effects on erosion rates.

The spatial patterns shown in the erosion maps were most likely due to the main factors found most sensitive in the sensitivity test (land cover, slope length, slope, and precipitation). Different combinations of these three factors provided a large range of yields which were amplified by the effects of extreme wildfire and climate change. The most influential factor causing the differences in yield was most likely land cover type because of its extreme sensitivity in the VIC-WEPP model.

The upscaling process in this study provides the capability and capacity to simulate mechanistic erosion processes at large scales even though erosion occurs fundamentally at very small scales. The random sampling approach was key to accurately describe the sediment yield within a VIC model grid cell and ultimately the entire basin. The current approach had important impacts that need to be investigated in much more detail. This includes the large percentage of erosion coming from cropland land cover type compared to the fractional area of the VIC model grid cell as shown in Chapter 5.

The changes in peak flow timing and magnitude for the future climate scenarios can provide insight into the potential adverse effects on water quality. Considering first the no fire severity condition, the peak flow day shifted one to two months earlier in the season as well as decreased peak flow magnitude. The shift could impact ecosystems negatively because aquatic life depend on consistent, seasonal streamflow for food (insects and vegetation may be absent with higher and faster

streamflow) and spawning (increased streamflow and sediment may change stream or river channel characterizes). Also, earlier flows may cause a shift in the temperature gradient of rivers and streams. Higher flows earlier in the season may cause lower streamflow temperatures (from snowmelt) and higher temperatures during the summer months because lower flows will increase in temperature faster. Along with the shift in streamflow, erosion changes can cause significant concerns for water management and ecosystems (dredging for example). Considering the climate impacts only, the shift in peak flow may cause sediment concentrations to increase earlier in the season potentially changing ecosystems that rely on smaller concentrations during that time of the year. With high fire severity conditions, the much larger flows may also be carrying a larger sediment load (USACE 2012). This has double the concern for reservoir managers that must manage the shift in streamflow timing and magnitude as well as increased sediment loads.

Due to the upscaling procedure, to select individual locations for erosion mitigations would not be directly helpful because a VIC model grid cell is approximately 35 $km^2$ and many mitigation techniques are not applied over such a large area. One different approach is to consider the erosion maps as erosion risk indication maps which take the land cover type, slope, and precipitation for an area and provides potential erosion relative to other areas. Instead of considering the impacts of these three variables separately, the erosion results incorporate them together in a physically-based model. These results may provide a manager something unexpected or new that before they would not have discovered.

# REFERENCES


Abatzoglou, J. T. 2011. Development of Gridded Surface Meteorological Data For Ecological Applications And Modeling. International Journal of Climatology. DOI: 10.1002/joc.3413.

Abatzoglou J. T. and T. J. Brown. 2011. A Comparison of Statistical Downscaling Methods Suited for Wildfire Applications. International Journal of Climatology. DOI: 10.1002/joc.2312.

Amaranthus, M. P. and J. M. Trappe. 1993. Effects of Erosion on Ecto- and VA-mycorrhizal Inoculum Potential of Soil Following Forest Fire in Southwest Oregon. Plant and Soil, Vol. 140, No. 1, pp 41-49.

Andreadis, K., P. Storck, and D. P. Lettenmaier. 2009. Modeling snow accumulation and ablation processes in forested environments. Water Resources Research, 45, W05429, doi:10.1029/2008WR007042.

Barsugli, J. J., M. M. Elsner, and A. F. Hamlet. 2012. Building a Stronger and More Extensive Hydrologic Foundation for Environmental Flow and Climate Change Research across the Colorado River Basin. Final report prepared for The Nature Conservancy.

Benavides-Solorio, J. D. and L. H. MacDonald. 2001. Post-fire runoff and erosion from simulated rainfall on small plots, Colorado Front Range. Hydrological Processes, Vol. 15, No. 15, pp 2931-2952.

Benavides-Solorio, J. D., and L. H. MacDonald. 2005. Measurement and prediction of post-fire erosion at the hillslope scale, Colorado Front Range. International Journal of Wildland Fire, Vol. 14, pp 457-474.

Benda, L., D. Miller, P. Bigelow, and K. Andras. 2003. Effects of post-wildfire erosion on channel environments, Boise River, Idaho. Forest Ecology and Management, Vol. 178, pp. 105-119.

Boll, J., E. Brooks, J. McAtty, M. Barber, J. Ullman, D. McCool, X. Lu, A. Lawler, and J. Ryan. 2011. Evaluation of sediment yield reduction potential in agricultural and mixed-use watersheds of the Lower Snake River basin. Technical Report, submitted to US Army Corps of Engineers by State of Washington Water Research Center, Pullman, WA.

Bowling, L. C. and D. P. Lettenmaier. 2010. Modeling the effects of lakes and wetlands on the water balance of Arctic environments. Journal of Hydrometeorology, Vol. 11, pp 276-295.

Bowling, L. C., J. W. Pomeroy, and D. P. Lettenmaier. 2004. Parameterization of blowing-snow sublimation in a macroscale hydrology model, J. Hydrometeorology, Vol. 5, pp 745-762.

Climate Change Science Program (CCSP) 2008. Weather and climate extremes in a changing climate. Regions of Focus: North America, Hawaii, Caribbean, and U.S. Pacific Islands. A Report by the U.S. Climate Change Science Program and the Subcommittee on Global Change

Research. [Thomas R. Karl, Gerald A. Meehl, Christopher D. Miller, Susan J. Hassol, Anne M. Waple, and William L. Murray (eds.)]. Department of Commerce, NOAA's National Climatic Data Center, Washington, D.C.

Cherkauer, K. A. and D. P. Lettenmaier. 1999. Hydrologic effects of frozen soils in the upper Mississippi River basin. Journal of Geophysical Research-Atmospheres, Vol. 104, pp 19599-19610.

Connaughton, C. A. 1935. Forest fires and accelerated erosion. Intermountain Forest and Range Experiment Station. Journal of Forestry, Vol. 33, No. 8, pp 751-752.

Coulibaly, P., B. Bobee, and F. Anctil. 2001. Improving extreme hydrologic events forecasting using a new criterion for artificial neural network selection. Hydrological Processes. 15: 1533-1536.

Daly C., M. Halbeib, J. I. Smith, W. P. Gibson, M. K. Doggett, G. H. Taylor, J. Curtis, and P. A. Pasteris. 2008. Physiographically-sensitive mapping of temperature and precipitation across the conterminous United States. International Journal of Climatology DOI: 10.1002/joc.1688.

Danielson, J. J., and D. B. Gesch. 2011. Global multi-resolution terrain elevation data 2010 (GMTED2010): U.S. Geological Survey Open-File Report 2011–1073, 26 p.

DeBano, L. F., D. G. Neary, and P. F. Folliott. 2005. Soil physical properties. In: D. G. Neary, K. C. Ryan, and L. F. DeBano, eds., Wildland fire in ecosystems: effects of fire on soils and water. U.S. Department of Agriculture, Forest Service, Rocky Mountain Research Station: General Technical Report, RMRS-GTR-42, pp 29-51. Ogden, UT.

Doerr, S. H., R. A. Shakesby, W. H. Blake, C. J. Chafer, G. S. Humphreys, and P. J. Walbrink. 2006. Effects of differing wildfire severities on soil wettability and implications for hydrological response. Journal of Hydrology, Vol. 319, pp 295-311.

Elliot, W. J. and D. E. Hall. 2010. Disturbed WEPP Model 2.0. Ver. 2011.11.22. Moscow, ID: U.S. Department of Agriculture, Forest Service, Rocky Mountain Research Station. Online at <http://forest.moscowfsl.wsu.edu/fswepp>.

Elliot, W. J., A. M. Liebenow, J. M. Laflen, and K. D. Kohl. 1989. A compendium of soil erodibility data from WEPP cropland soil field erodibility experiments 1987 & 1988, NSERL Report no.3, USDA-ARS National Soil Erosion Research Laboratory, West Lafayette, IN.

Elliot, W. J., R. B. Foltz, and S. Miller. 2010. Upland erosion processes in northern Idaho forests (Draft report). U.S. Forest Service, Rocky Mountain Research Station, Moscow, ID.

Elsner, M., L. Cuo, N. Voisin, J. Deems, A. Hamlet, J. Vano, K. Mickelson, S.-Y. Lee, and D. Lettenmaier. 2010. Implications of 21st century climate change for the hydrology of Washington State, Climatic Change, 102(1), 225-260.

Espinosa, F. A., J. J. Rhodes, and D. A. McCullough. 1997. The failure of existing plans to protect samon habiata in the Clearwater National Forest in Idaho. Journal of Environmental Management, Vol. 49, pp 205-230.

Flanagan, D. C. and M. A. Nearing. 1995. USDA – Water Erosion Prediction Project: Hillslope Profile and Watershed Model Documentation, West Lafayette, IN.

Flanagan, D. C., G. R. Foster, and W. C. Moldenhauer. 1987. How storm patterns affect infiltration, paper presented at Proc. International Conference on Infiltration Development and Application, University of Hawaii, Water Resources Research Center, Honolulu, HI, Jan 6–9, 1987.

Flanagan, D. C., J. C. Ascough, W. F. Geter, and O. David. 2005. Development of a hillslope erosion module for the object modeling system, paper presented at ASAE Annual International Meeting, Tampa, FL., ASAE, St. Joseph, MI, July 17-20.

Foster, G.R., D.C. Yoder, D.K. McCool, G.A. Weesies, T.J. Toy, L.E. Wagner. 2000. Improvements in science in RUSLE2. Paper No. 00-2147. ASAE, 2950 Niles Rd., St. Joseph, MI 439085-9659 USA.

Frankenberger, J. R., S. Dun, D. C. Flanagan, J. Q. Wu, W. J. Elliot. 2011. Development of a GIS Interface for WEPP Model Application to Great Lakes Forested Watersheds. Presented at the International Symposium on Erosion and Landscape Evolution. Anchorage, Alaska. ISELE Paper Number 11139.

Friedl, M. A., D. K. McIver, J. C. F. Hodges, X. Y. Zhang, D. Muchoney, A. H. Strahler, C. E. Woodcock, S. Gopal, A. Schneider, A. Cooper, A. Baccini, F. Gao, and C. Schaaf. 2002. Global land cover mapping from MODIS: Algorithms and early results, Remote Sensing of Environment, 83, 287–302.

Gao, H., Q. Tang, X. Shi, C. Zhu, T. J. Bohn, F. Su, J. Sheffield, M. Pan, D. P. Lettenmaier, and E. F. Wood. 2010. Water Budget Record from Variable Infiltration Capacity (VIC) Model. In Algorithm Theoretical Basis Document for Terrestrial Water Cycle Data Records (in review).

Goode, J. R., C. H. Luce, and J. M. Buffington. 2012. Enhanced sediment delivery in a changing climate in semi-arid mountain basins: Implications for water resource management and aquatic habitat in the northern Rocky Mountains. Geomorphology 139-140: 1-15.

Hamlet, A. F. and D. P. Lettenmaier. 1999. Effects of climate change on hydrology and water resources in the Columbia river basin, Journal of the American Water Resources Association, Vol. 35, pp 1597-1623.

Hamlet, A. F., M. M. Elsner, G. Mauger, S.-Y. Lee, and I. Tohver. 2012. An overview of the Columbia Basin Climate Change Scenarios Project: Approach, methods, and summary of key results. Atmosphere-Ocean, (in review).

Hann, W.J., D. G. Long, and J. P. Menakis. 1997. Landscape Ecology Assessment and Evaluation of Alternatives Data Analysis Record. USDA, Forest Service, USDI Bureau of Land Management, Interior Columbia Basin Ecosystem Management Project, 112 E: Poplar, Walla Walla: WA 99362.

Helvey, J. D. 1980. Effects of a north central Washington wildfire on runoff and sediment production. Journal of the American Water Resources Association, Vol. 16, No. 4, pp 627-634.

Holden, Z. A., P. Morgan, C. Luce, M. Crimmins, and E. Heyerdahl. 2006. Sensitivity of recent wildfire extent and severity to annual streamflow distribution and timing in the Pacific Northwest USA (1984-2005). The Journal of the Association for Fire Ecology.

Inbar, M., M. Tamir, and L. Wittenberg. 1998. Runoff and erosion processes after a forest fire in Mount Carmel, a Mediterranean area. Geomorphology, Vol. 24, No. 1, pp 17-33.

International Panel on Climate Change (IPCC). 2007. Climate Change 2007: Impacts, adaptation, and vulnerability. Contribution of Working Group II to the Fourth Assessment Report of the Intergovernmental Panel on Climate Change [Parry, Martin L., Canziani, Osvaldo F., Palutikof, Jean P., van der Linden, Paul J., and Hanson, Clair E. (eds.)]. Cambridge University Press, Cambridge, United Kingdom, 1000 pp.

Jetten, V., A. de Roo, and D. Favis-Mortlock. 1999. Evaluation of field-scale and catchment-scale soil erosion models. Catena 37 (3-4), 521-541.

Johansen, M. P., T. E. Hokonson, and D. D. Breshears. 2001. Post-fire runoff and erosion from rainfall simulation: contrasting forests with shrublands and grasslands. Hydrological Processes, Vol. 15, No. 15, pp 2953-2965.

Kandel, D. D., A. W. Western, R. B. Grayson, and H. N. Turral (2004), Process parameterization and temporal scaling in surface runoff and erosion modeling, Hydrologic Processes, 18, 1423–1446.

Kirchner, J. W., R. C. Finkel, C. S. Riebe, D. E. Granger, J. L. Clayton, J. G. King, and W. F. Megahan. 2001. Mountain erosion over 10 yr, 10 k.y., and 10 m.y. time scales. Geology, 29(7): 591-594.

Kirschbaum, R.L., and D. P. Lettenmaier. 1997. An Evaluation of the Effects of Anthropogenic Activity on Streamflow in the Columbia River Basin. University of Washington, Department of Civil Engineering, Water Resources Series Tech. Rep. No. 156: Seattle, WA.

Kunkel, M. L., and J. L. Pierce. 2010. Reconstructing snowmelt in Idaho's watershed using historic streamflow records. Climatic Change, v. 98, no. 1-2, p. 155-176. 10.1007/s10584-009-9651-x.

Laflen, G. A., J. M. Elliot, W. J. Simanton, J. R. Holzhey, C. S. and K. D. Kohl. 1991. WEPP: Soil erodibility experiments for rangeland and cropland soils. Journal of Soil and Water Conservation, 46(1), 39-44.

Larsen, I. J., L. H. MacDonald, E. Brown, D. Rough, M. J. Welsh, J. H. Pietraszek, Z. Libohova, J. D. Benavides-Solorio, and K. Schaffrath. 2009. Causes of post-fire runoff and erosion: water repellency, cover, or soil sealing? Soil Science Society of America Journal, Vol. 73, pp 1393-1407.

Liang, X., D. P. Lettenmaier, E. Wood, and S. J. Burges. 1994. A simple hydrologically based model of land-surface water and energy fluxes for general-circulation models. Journal of Geophysical Research-Atmospheres, Vol. 99, pp 14415-14428.

Lohmann, D., R. Nolte-Holube, and E. Raschke. 1996. A large-scale horizontal routing model to be coupled to land surface parametrization schemes. Tellus 48(A), 708-721.

Lohmann, D., E. Raschke, B. Nijssen and D. P. Lettenmaier. 1998. Regional scale hydrology: I. Formulation of the VIC-2L model coupled to a routing model. Hydrological Sciences Journal 43(1), 131-141.

Loveland, T.R., J. M. Merchant, D. O. Ohlen, and J. F. Brown. 1991. Development of a land-cover characteristics database for the coterminous US. Photogrammetric Engineering and Remote Sensing, 57: 1453-1463.

Loveland, T.R., and D. O. Ohlen. 1993. Experimental AVHRR land data sets for environmental monitoring and modelling. In Environmental Modelling with GIS. M. F. Goodchild, B. O. Parks, L. T. Steyaert (eds); Oxford University Press: New York; 379-385.

Lown, J.B., J.P. Lyon, D.C. Yoder. 2000. A Scientific Modeling Architecture to Simultaneously Meet Needs of Scientists, Programmers, Data Managers, and End-Users. Paper No. 003051. ASAE, 2950 Niles Rd., St. Joseph, MI 439085-9659 USA.

Mao, D., K. A. Cherkauer, and D. C. Flanagan. 2010. Development of a coupled soil erosion and large-scale hydrology modeling system. Water Resources Research, 46, W08543, doi: 10.1029/2009WR008268.

Matheussen, B., R. Kirschbaum, I. Goodman, G. O'Donnell, and D. Lettenmaier. 2000. Effects of land cover change on streamflow in the interior Columbia River Basin (USA and Canada). Hydrologic Processes, 14(5), 867–885.

Maurer, E. P., A. W. Wood, J. C. Adam, D. P. Lettenmaier, and B. Nijssen. 2002. A long-term hydrologically-based data set of land surface fluxes and states for the conterminous United States. Journal of Climate, Vol. 15, pp 3237-3251.

McCutcheon, S. C. and J. Pendergast. 1999. Overview of total maximum daily load (TMDL) problem and supporting model development. Presented at Appalachian Rivers II Conference, Morgantown, WV.

Menakis, J.P., D. G. Long, and R. E. Keane. 1996. The development of key broad-scale layers and characterization files. In Compilation of Administrative Reports: Multi-scale Landscape Dynamics in the Basin and Portions of the Klamath and Great basins. R. E. Keane, J. L. Jones, L. S. Riley, W. J. Hann (Eds). USDA, Forest Service, USDI, Bureau of Land Management, Interior Columbia Basin Ecosystem Management Project, 112 E: Poplar, Walla Walla: WA 99362.

Minshall, G. W. and J. T. Brock.1991. Observed and anticipated effects of forest fire on Yellowstone stream ecosystems. Chapter 10 in The Greater Yellowstone Ecosystem, edited by R.B. Keiter and M.S. Boyce, Yale University.

Mitchell, K. E., D. Lohmann, P. R. Houser, E. F. Wood, J. C. Schaake, A. Robock, B. A. Cosgrove, J. Sheffield, Q. Duan, L. Luo, R. W. Higgins, R. T. Pinker, J. D. Tarpley, D. P. Lettenmaier, C. H. Marshall, J. K. Entin, M. Pan, W. Shi, V. Koren, J. Meng, B. H. Ramsay, and A. A. Bailey. 2004. The multi-institution North American Land Data Assimilation System (NLDAS): Utilizing multiple GCIP products and partners in a continental distributed hydrological modeling system. Journal of Geophysical Research, Vol. 109: D07S90, DOI: 10.1029/2003JD003823.

Moody, J. A. and D. A. Martin. 2001. Initial hydrologic and geomorphic response following a wildfire in the Colorado Front Range. Earth Surface Processes and Landforms, Vol. 26, pp 1049-1070.

Moody, J. A. and D. A. Martin. 2009. Synthesis of sediment yields after wildland fire in different rainfall regimes in the western United States. International Journal of Wildland Fire, Vol. 18, pp 96-115.

Moriasi, D. N., J. G. Arnold, M. W. Van Liew, R. L. Bingner, R. D. Harmel, and T. L. Veith. 2007. Model Evaluation Guidelines for Systematic Quantification of Accuracy in Watershed Simulations. Transactions of the American Society of Agricultural and Biological Engineers, 50 (3), 885–900.

Moss, R. H., J. A. Edmonds, K. A. Hibbard, M. R. Manning, S. K. Rose, D. P. van Vuuren, T.R. Carter, S. Emori, M. Kainuma, T. Kram, et al. 2010. The next generation of scenarios for climate change research and assessment. Nature 463:747–756.

Nicks, A. D., L. J. Lane, and G. A. Gander. 1995. Weather generator, in USDA-Water Erosion Prediction Project: Hillslope Profile and Watershed Model Documentation, edited by D. C. Flanagan and M. A. Nearing, pp. 2.1–2.2, USDA-ARS National Soil Erosion Research Laboratory, West Lafayette, IN.

Nijssen B., D. P. Lettenmaier, X. Liang, S. W. Wetzel, and E. F. Wood. 1997. Streamflow simulation for continental-scale river basins. Water Resources Research 33(4): 711-724.

Owens, P. N., R. J. Batalla, A. J. Collins, B. Gomez, D. M. Hicks, A. J. Horowitz, G. M. Kondolf, M. Marden, M. J. Page, D. H. Peacock, E. L. Petticrew, W. Salomons, and N. A. Trustrum. 2005. Fine-grained sediment in river systems: environmental significance and management issues. River Research and Applications, Vol. 21, No. 7, pp 693-717.

Park, S. J., and N. Van de Giesen. 2004. Soil-landscape delineation to define spatial sampling domains for hillslope hydrology. Journal of Hydrology, 295, 28–46.

Parson A., P. R. Robichaud, S. A. Lewis, C. Napper, and J. T. Clark. 2010. Field guide for mapping post-fire soil burn severity. Gen. Tech. Rep. RMRS-GTR-243. Fort Collins, CO. U.S. Department of Agriculture, Forest Service, Rocky Mountain Research Station. pp 49.

Quigley, T. M., and S. J. Arbelide (Eds). 1997. An Assessment of the Ecosystem Components in the Interior Columbia Basin and Portions of the Klamath and Great Basins. Vol. 2, General Technical Report, PNW-GTR-405. Portland, OR.

Renard, G. K., G. R. Foster, G. A. Weesies, and J. P. Porter. 1991. RUSLE - Revised universal soil loss equation. Journal of Soil and Water Conservation, v. 46, p.30-33.

Reneau, S. L., D. Katzman, G.A. Kuyumjian, A. Lavine, and D. V. Malmon. 2010. Sediment delivery after a wildfire. Geology, Vol. 35, pp. 151-154.

Robertson, M. J., D. A. Scruton, and K. D. Clarke. 2007. Seasonal effects of suspended sediment on the behavior of juvenile Atlantic salmon. Transactions of the American Fisheries Society, Vol. 136, pp 822-828.

Robichaud, P. R. 2000. Fire effects on infiltration rates after prescribed fire in northern Rocky Mountain forests, USA. Journal of Hydrology, Vol. 231-232, pp 220–229.

Robichaud, P. R., W. J. Elliot, F. B. Pierson, D. E. Hill, and C. A. Moffet, 2007. Predicting postfire erosion and mitigation effectiveness with a web-based probabilistic erosion model. Catena 71 (2), 229-241.

Robichaud, P. R., J. W. Wagenbrenner and R. E. Brown. 2010. Rill erosion in natural and disturbed forests: 1. Measurements. Water Resources Research, Vol. 46, W10506.

Schubauer-Berigan, J. P., S. Minamyer, and E. Hartzell. 2005. Proceedings of a workshop on suspended sediments and solids. EPA/600/R-06/025, U.S. EPA Office of Research and Development, Cincinnati, OH.

Spigel, K. M. and Robichaud, P. R. 2007. First-year post-fire erosion rates in Bitterroot National Forest, Montana. Hydrological Processes. 21: 998-1005.

Sridhar, V., X. Jin, and W. T. Jaksa. 2012. Explaining the hydroclimatic variability and change in the Salmon River basin. Climate Dynamics, DOI 10.1007/s00382-012-1467-0.

Tang, C., B. T. Crosby, J. M. Wheaton, and T. C. Piechota. 2012. Assessing streamflow sensitivity to temperature increases in the Salmon River Basin, Idaho. Journal of Global and Planetary Change, 88-89 - 32-44.

Teasdale, G. N. and M. E. Barber. 2008. Aerial Assessment of Ephemeral Gully Erosion from Agricultural Regions in the Pacific Northwest. ASCE Journal of Irrigation and Drainage Engineering, Vol. 134, No. 6, pp 807-814.

Tetra Tech EC, Inc. (Tetra Tech). 2006. Investigation of Sediment Source and Yield, Management, and Restoration Opportunities within the Lower Snake River Basin. Contract W912EF-05-D-002, U.S. Army Corps of Engineers, Walla Walla District, April, 2006, Thurow, R.

Thompson, J. A., E. M. Pena-Yewtukhiw, and J. H. Grove. 2006. Soil landscape modeling across a physiographic region: Topographic patterns and model transportability, Geoderma, 133, 57–70.

U.S. Army Corps of Engineers (USACE). 2011a. Lower Granite Reservoir – Hydrologic and Hydraulic Investigations. Draft, U.S. Army Corps of Engineers Walla Walla District, May, 2011.

U.S. Army Corps of Engineers (USACE). 2012. Lower Snake River Programmatic Sediment Management Plan/Environmental Impact Statement. Draft, U.S. Army Corps of Engineers Walla Walla District, December 2012.

United States Department of Agriculture (USDA). 1994. State Soil Geographic (STATSGO) Data Base Ð Data Use Information, Miscellaneous Publication No. 1492 (revised edition). US Department of Agriculture, National Resources Conservation Service: Forth Worth, Texas.

United States Department of Agriculture (USDA). 2012. WEPP Release Notes. Retrieved June 16, 2013, from Agricultural Research Service: http://www.ars.usda.gov/Research/docs.htm?docid=18082

Westerling, A. L., H. G. Hidalgo, D. R. Cayan, and T. W. Swetnam. 2006. Warming and earlier spring increase western U.S. forest wildfire activity. Science, 313(5789):940-943.

Williams, J. R. and H. D. Berndt. 1977. Sediment yield prediction based on watershed hydrology. Transactions of the American Society of Agricultural Engineers, 20(6): 1100–1104.

Wischmeier, W. H., and D. D. Smith. 1978. Predicting rainfall erosion losses - a guide to conservation planning, Agr. Handbk. No. 537. U.S. Dept. Agr., Washington, D.C.

Wood, P. J. and P. D. Armitage. 1997. Biological effects of fine sediment in the lotic environment. Environmental Management, 21(2):203-217.

Zhang, X. C., and J. D. Garbrecht. 2003. Evaluation of CLIGEN precipitation parameters and their implication on WEPP runoff and erosion prediction. Transactions of the American Society of Agricultural Engineers, 46(2), 311–320.

# APPENDIX

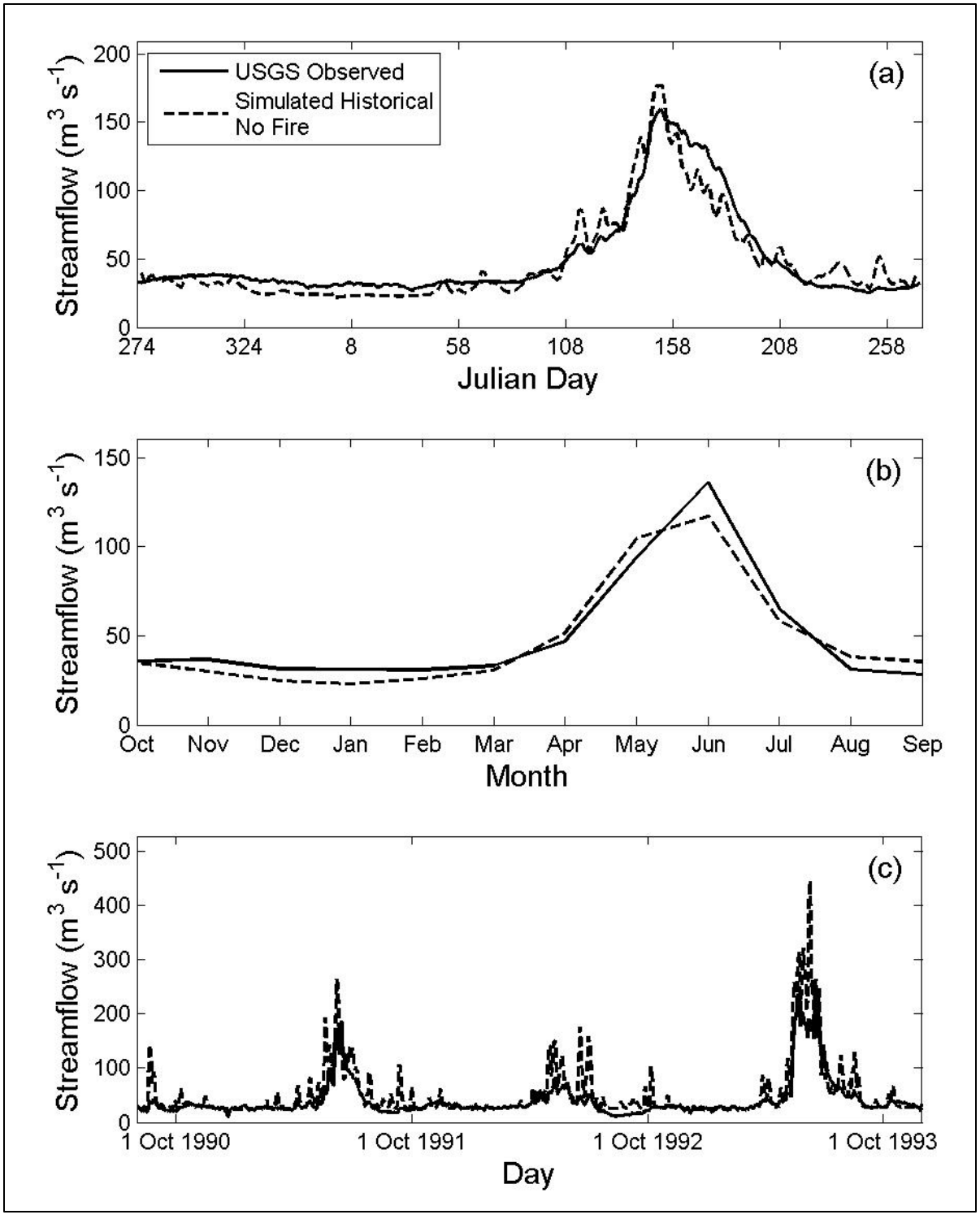


Figure 19. Observed and calibrated simulated discharge at the outlet of Basin Two for (a) the average Julian day, (b) average month, and (c) three years of daily flows.

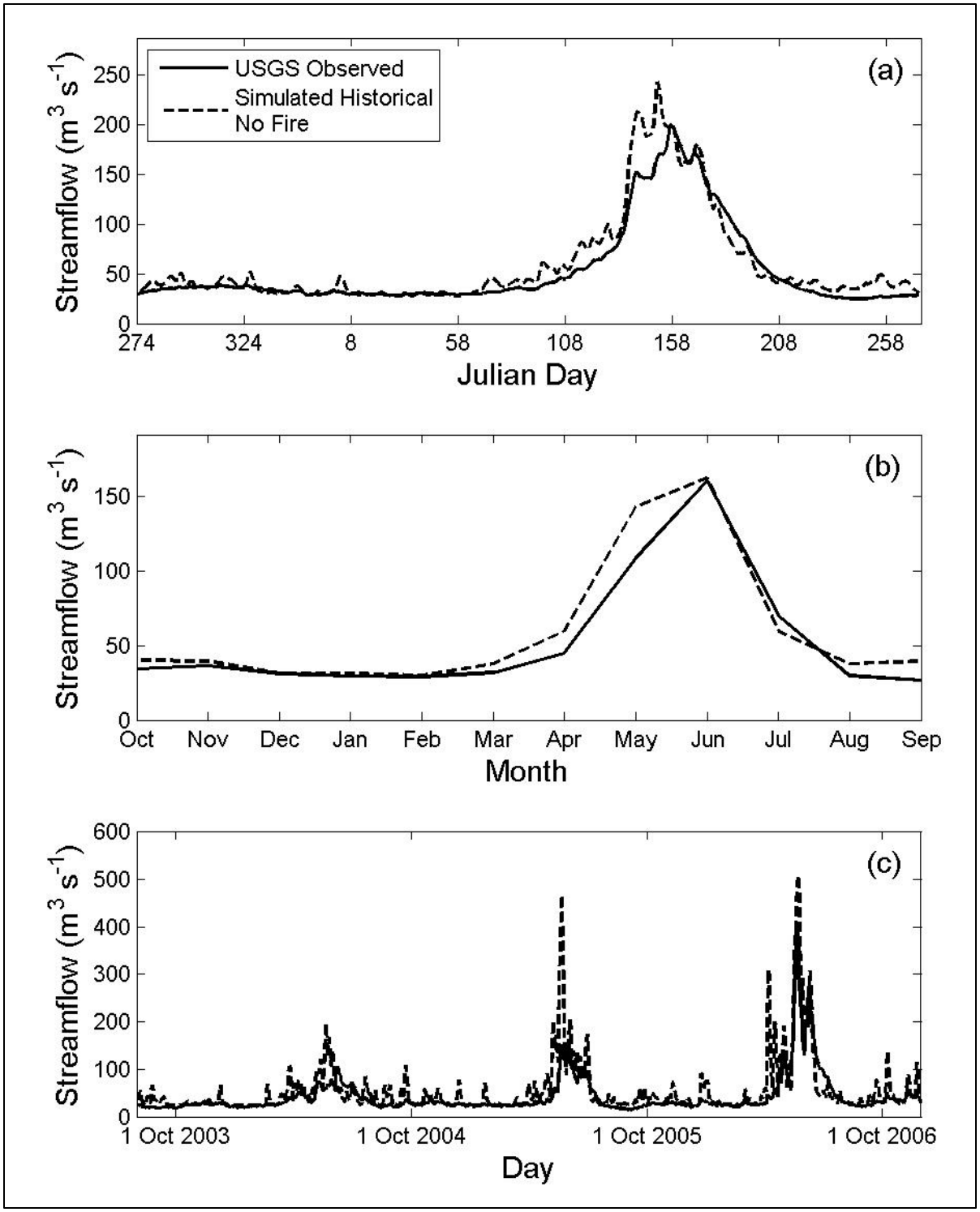


Figure 20. Observed and evaluated simulated discharge at the outlet of Basin Two for (a) the average Julian day, (b) average month, and (c) three years of daily flows.

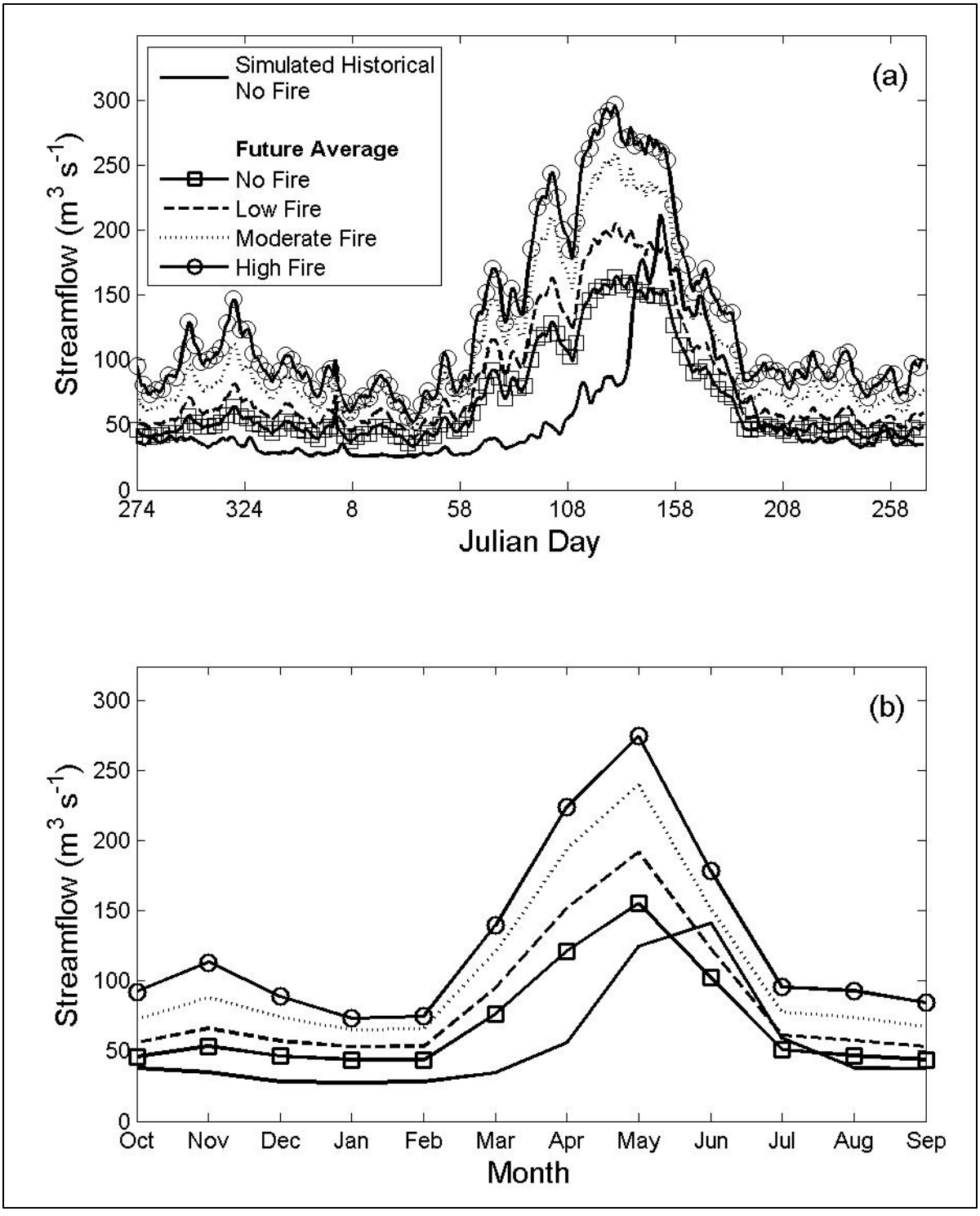


Figure 21. Future streamflow compared to historical simulated streamflow for no, low, moderate, and high fire severity conditions for Basin Two for (a) the average Julian day streamflow (beginning on October 1) and (b) the average monthly streamflow. The future streamflow is the average of the five future scenarios (see Section 3.5).

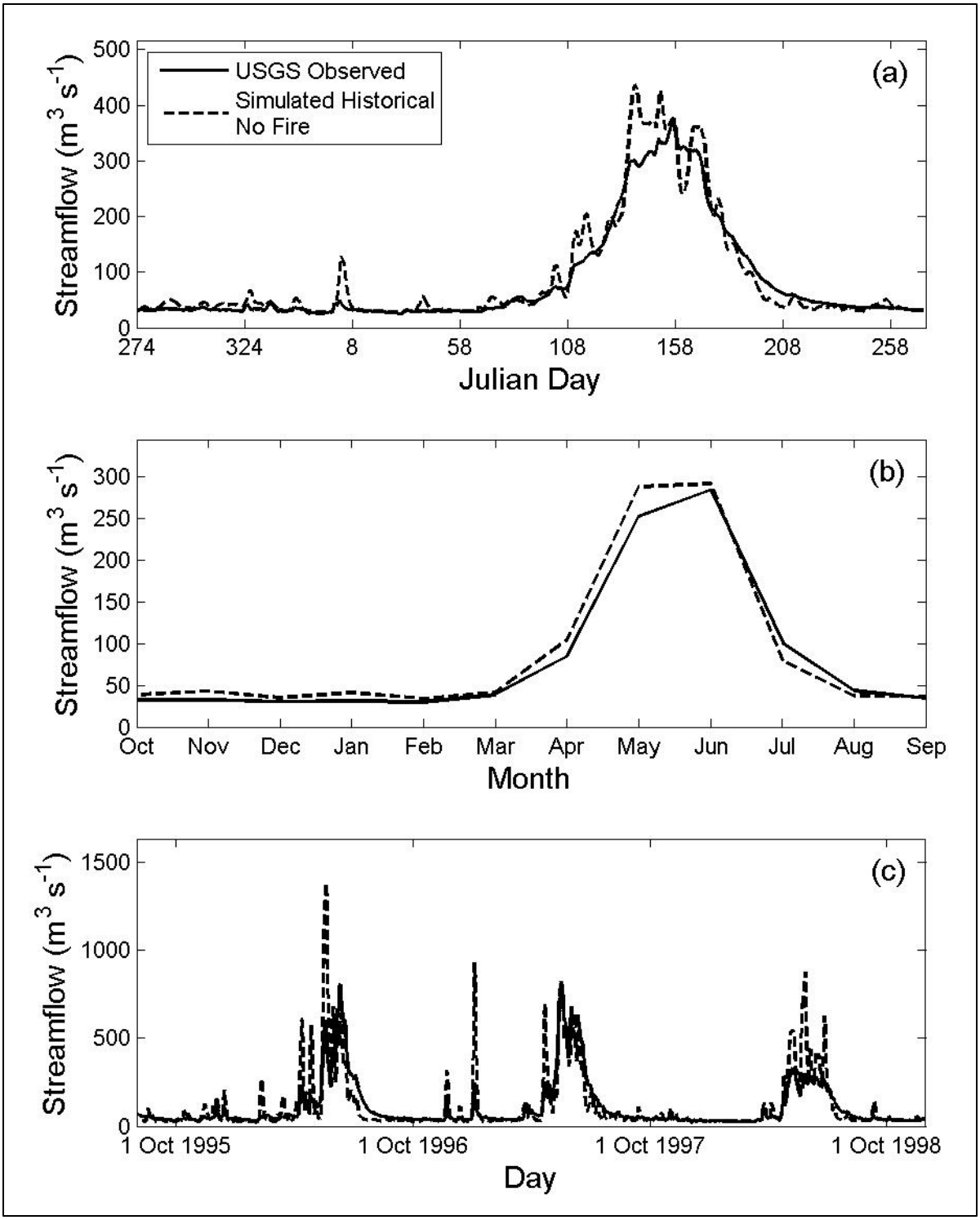


Figure 22. Observed and calibrated simulated discharge at the outlet of Basin Three for (a) the average Julian day, (b) average month, and (c) three years of daily flows.

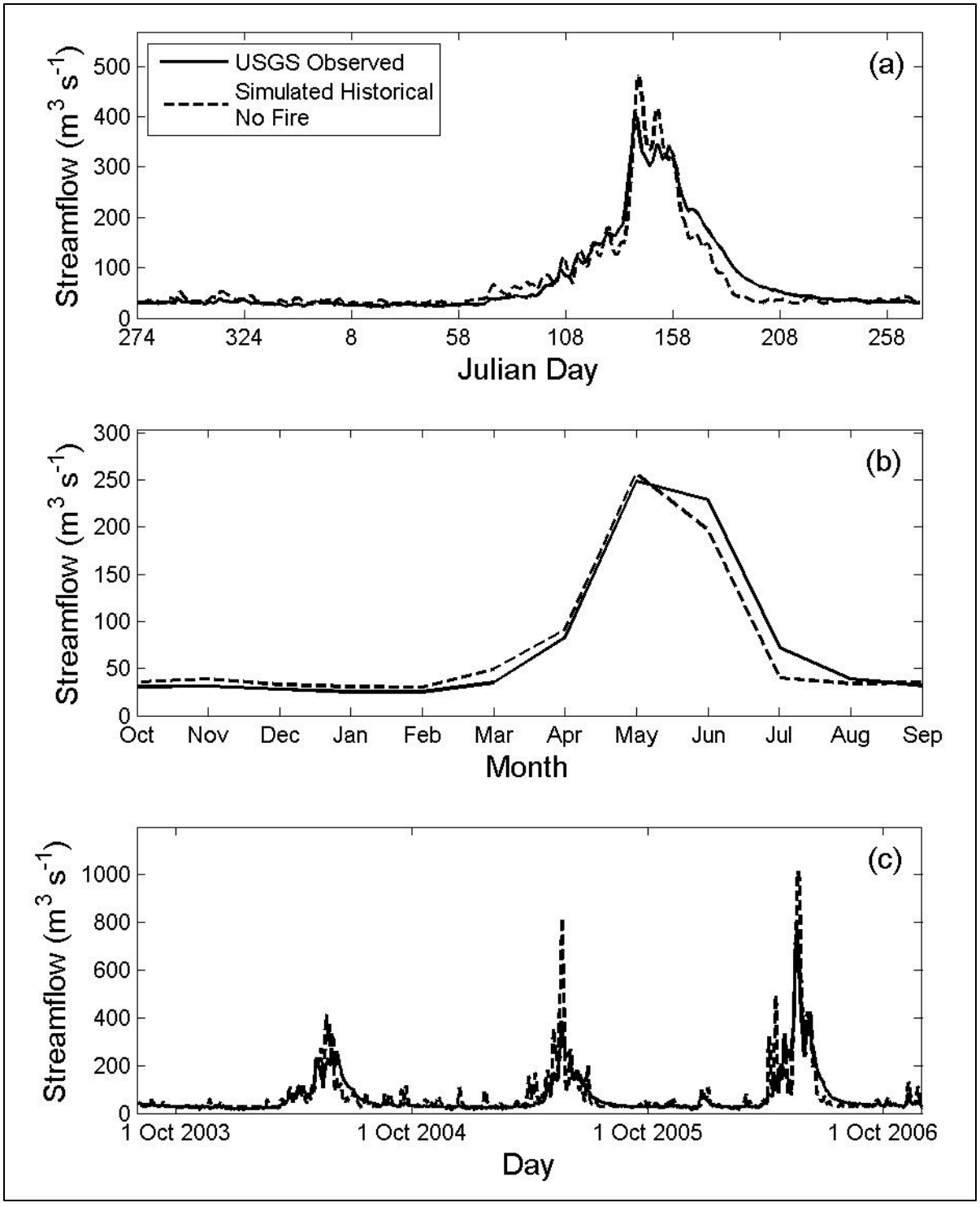


Figure 23. Observed and evaluated simulated discharge at the outlet of Basin Three for (a) the average Julian day, (b) average month, and (c) three years of daily flows.

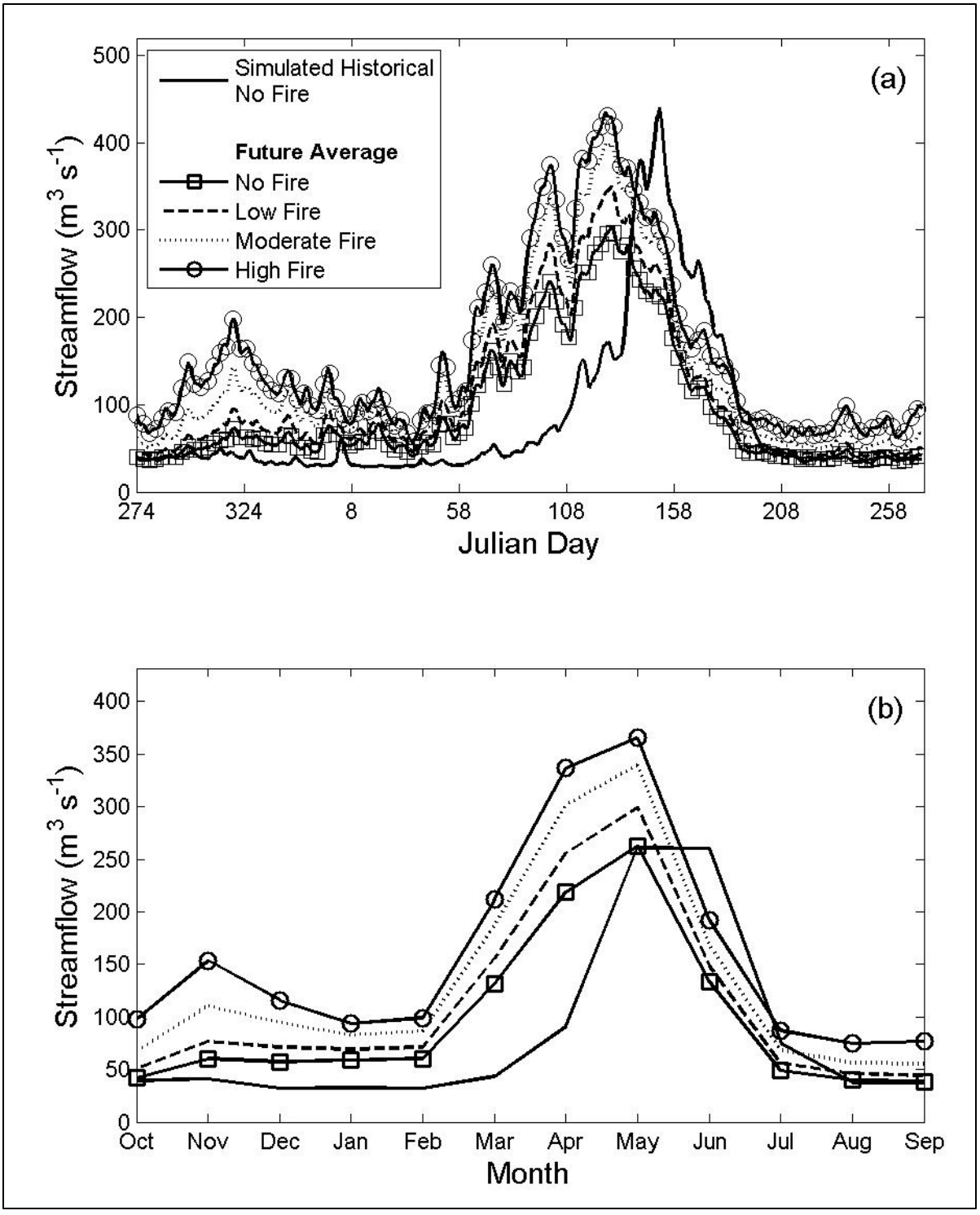


Figure 24. Future streamflow compared to historical simulated streamflow for no, low, moderate, and high fire severity conditions for Basin Three for (a) the average Julian day streamflow (beginning on October 1) and (b) the average monthly streamflow. The future streamflow is the average of the five future scenarios (see Section 3.5).

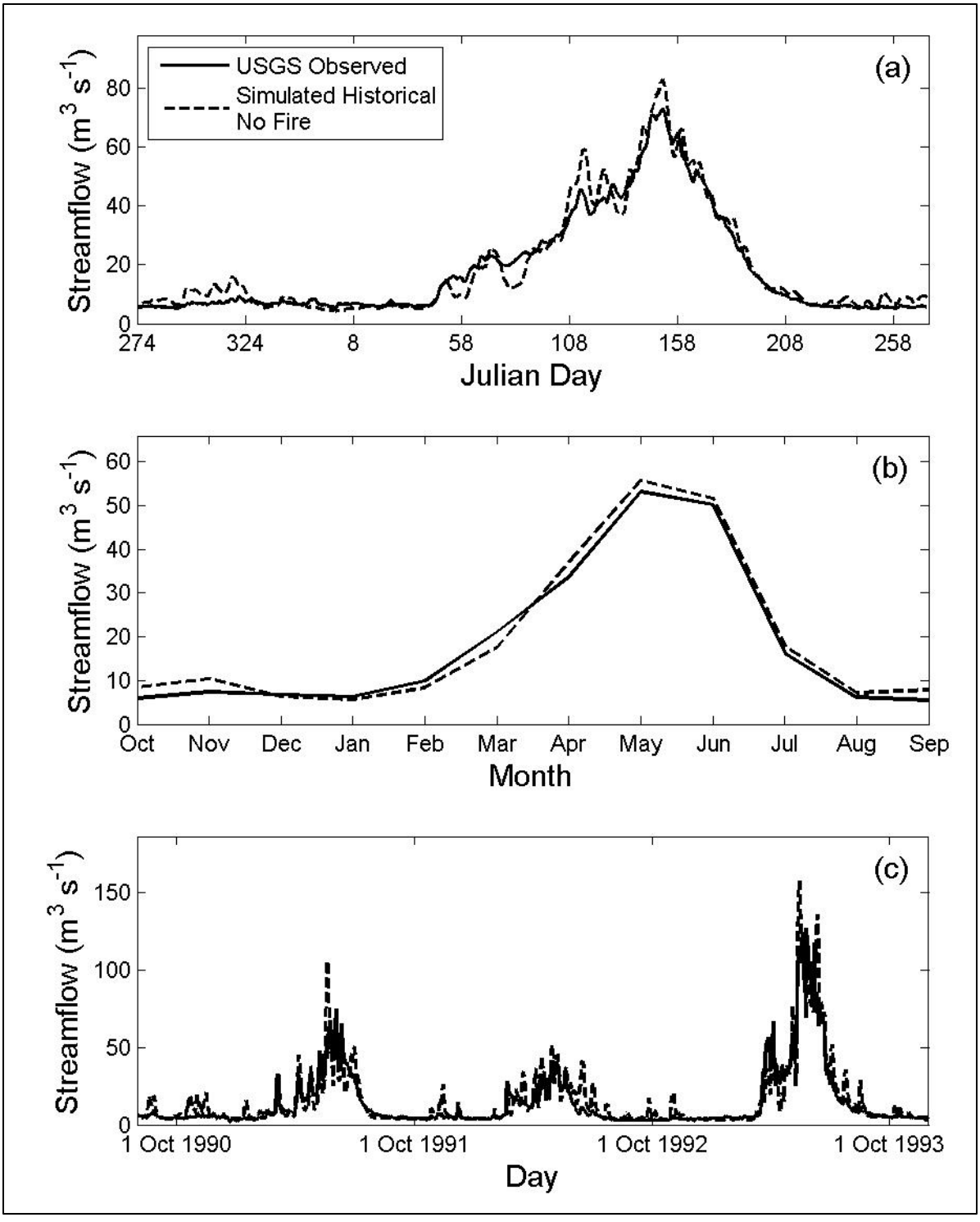


Figure 25. Observed and calibrated simulated discharge at the outlet of Basin Four for (a) the average Julian day, (b) average month, and (c) three years of daily flows.

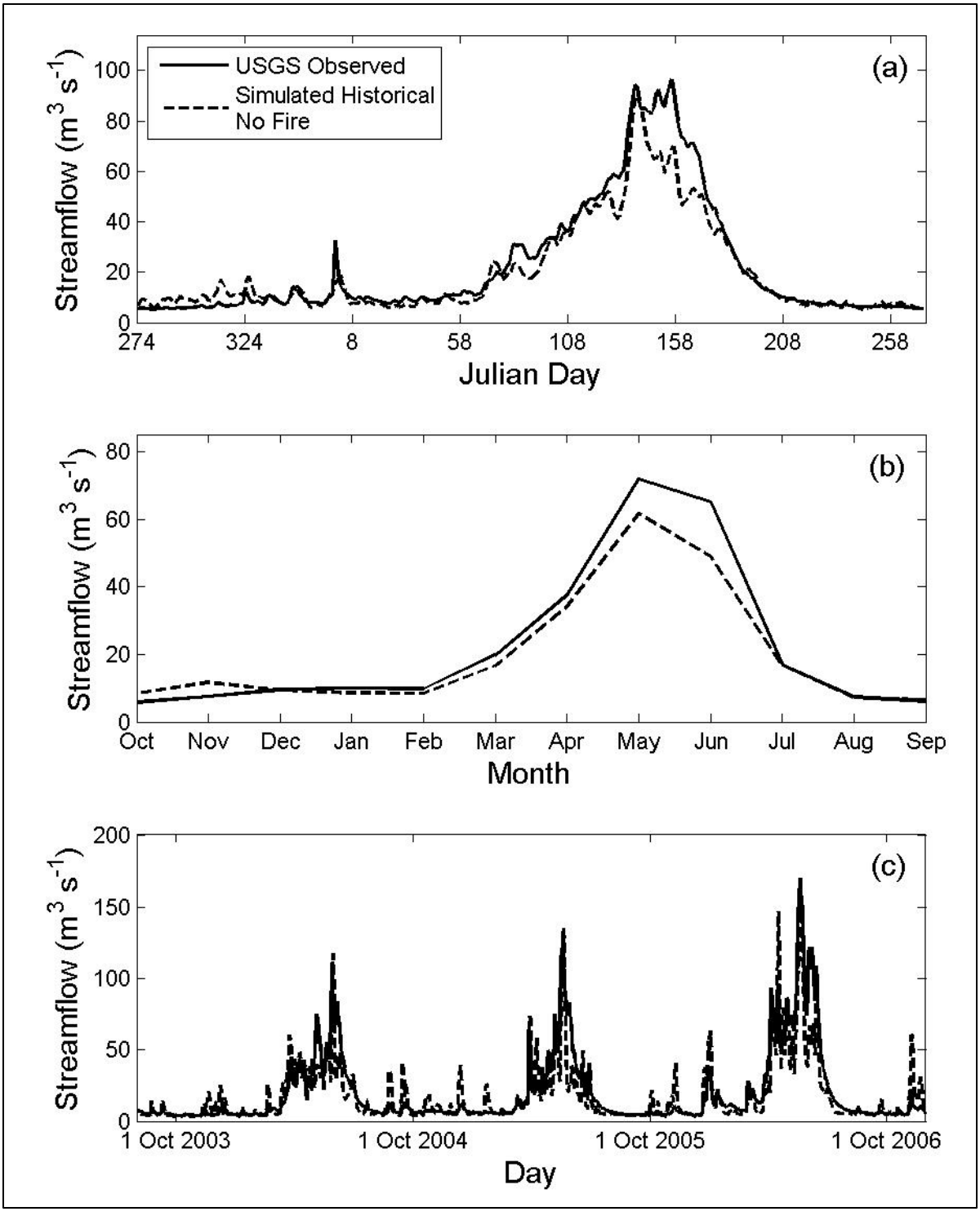


Figure 26. Observed and evaluated simulated discharge at the outlet of Basin Four for (a) the average Julian day, (b) average month, and (c) three years of daily flows.

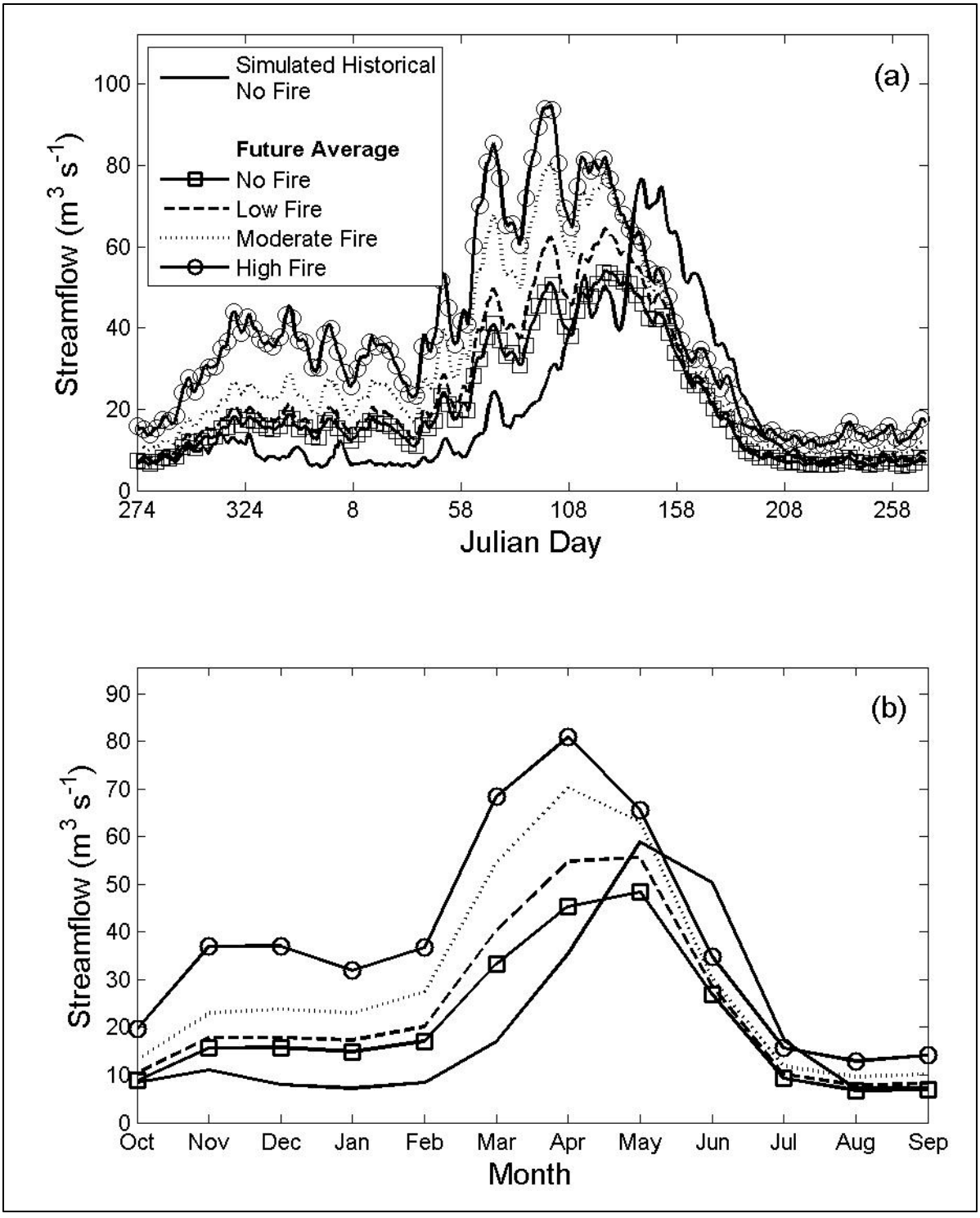


Figure 27. Future streamflow compared to historical simulated streamflow for no, low, moderate, and high fire severity conditions for Basin Four for (a) the average Julian day streamflow (beginning on October 1) and (b) the average monthly streamflow. The future streamflow is the average of the five future scenarios (see Section 3.5).